General Disclaimer

One or more of the Following Statements may affect this Document

- This document has been reproduced from the best copy furnished by the organizational source. It is being released in the interest of making available as much information as possible.

- This document may contain data, which exceeds the sheet parameters. It was furnished in this condition by the organizational source and is the best copy available.

- This document may contain tone-on-tone or color graphs, charts and/or pictures, which have been reproduced in black and white.

- This document is paginated as submitted by the original source.

- Portions of this document are not fully legible due to the historical nature of some of the material. However, it is the best reproduction available from the original submission.

7.7-10012
CR-148982

MULTISPECTRAL CHARACTERISTICS OF CLOUDS OBSERVED BY LANDSAT 2

(E77-10012) MESOSCALE ASSESSMENTS OF CLOUD AND RAINFALL OVER THE BRITISH ISLES (Department of Industry) 53 p HC A04/MF A01 CSCL 04B
N77-10594
Unclas
G3/43 00012

ERTS Follow-on Programme Study No. 2962A

Fourth Quarterly Report on

Mesoscale Assessments of Cloud and Rainfall

over the British Isles

by

Eric C. Barrett
M.Sc., Ph.D., F.R.G.S., F.R.Met.S., F.B.I.S.

Colin K. Grant
B.Sc., F.R.Met.S.

and

R. Harris
B.A., F.R.Met.S.

Supported by the U.K. Department of Industry,
Monsanto House, 10-18 Victoria Street, London, SW1H ONQ.

September 1976.

MULTISPECTRAL CHARACTERISTICS OF CLOUDS OBSERVED BY LANDSAT 2

ERTS Follow-on Programme Study No. 2962A

Fourth Quarterly Report on Mesoscale Assessments of Cloud and Rainfall over the British Isles

by

Eric C. Barrett
M.Sc., Ph.D., F.R.G.S., F.R.Met.S., F.B.I.S.

Colin K. Grant
B.Sc., F.R.Met.S.

and

R. Harris
B.A., F.R.Met.S.

Supported by the U.K. Department of Industry,
Monsanto House, 10-18 Victoria Street, London, SW1H ONQ.

September 1976.

CONTENTS

I INTRODUCTION

In our two previous reports attention was paid to the compilation of cloud photointerpretation keys for Landsat imagery so that the recognition of various cloud types might be put on a firm footing (Barrett and Grant, 1976a), and eyeball and machine-assisted comparisons were made between estimates of cloud cover imaged by Landsat and observed from the ground (Barrett and Grant, 1976b). This latter work included the development of an appropriate methodology, and the compilation of some initial results. In due course it is intended that these results should be supplemented by others for that portion of the study period for which imagery had not become available (generally February and March, 1976). Since we had not received our final consignments of images by mid-August 1976 the completion of that part of our exercise has still to be effected. Table 1 and Figure 1 indicate the frames received since the preparation of the Third Quarterly Report; Figure 2 displays the distribution through time of our entire archive of images as it stands at the time of writing.

It was thought convenient, whilst we were awaiting the remainder of the images for our study period, to experiment with a further section of our work which seeks to evaluate Landsat cloud images in comparison with those from other satellite families. This section is concerned with simultaneous analyses of data in all four Landsat multispectral sensor wavebands, leading to an appreciation of the suitability of the Landsat MSS wavebands for cloud analysis and identification. Many studies have considered the multispectral responses of Landsat-viewed surface-features; many more have considered the significance of multispectral data for differentiating both between and within classes of a wide variety of surface features (see e.g. NASA, 1975). However, we are unaware of detailed studies of the multispectral characteristics of Landsat-viewed clouds, though Danko (1974) addressed himself in part to this question.

LANDSAT COVERAGE OF THE BRITISH ISLES:

Tabulation of Individual Frames

(see also Table 2 in Barrett and Grant, 1975(b), Table 1 in Barrett and Grant 1976(a), and Table 1 in Barrett and Grant 1976 (b)).

DAY Since Launch	DATE (1975)	ORBIT NUMBER	Frame Numbers 4 6	Frame Numbers 5 7	TIME H : M : S	CO-ORDS OF CENTRE LATITUDE	CO-ORDS OF CENTRE LONGITUDE
2323	11 DECEMBER	4500	008	025	11:06:00	N 54:34	W011:19
			042	059			
			009	026	11:06:30	N53 10	W012:07
			043	060			
2338	26 DECEMBER	4709	061	097	10:49:10	N 53:08	W007:53
			133	169			
			062	098	10:49:30	N 51:43	W008:36
			134	170			
			063	099	10:50:00	N50:18	W009:17
			135	171			
			064	100	10:50 20	N48:53	W009:56
			136	172			
	1976						
2347	4 JANUARY	4834	229	242	09:58:10	N50: 11	E003:33
			255	268			
			230	243	09:58:40	N48:46	E002:54
			256	269			
2354	11 JANUARY	4932	008	038	10:37:00	N54:18	W004:24
			068	098			
			009	039	10:37:30	N52:54	W005:09
			069	099			
			010	040	10:37:50	N51:30	W005:51
			070	100			
			011	041	10:38:20	N50:06	W006:32
			071	101			
2355	12 JANUARY	4946	006	037	10:42:50	N54:19	W005:50
			MSG	099			
			007	038	10:43:10	N52:55	W006:35
			MSG	100			
			008	039	10:43:40	N51:31	W007:18
			MSG	101			
			009	040	10:44:00	N50:07	W007:58
			MSG	102			
			010	041	10:44:30	N48:42	W008:37
			MSG	103			
2357	14 JANUARY	4974	066	081	10:55:30	N50:10	W010:48
			096	111			
			067	082	10:55:50	N48:45	W011:27
			097	112			
2358	15 JANUARY	4988	010	024	11:01:40	N48:44	W012:53
			038	052			

DAY Since Launch	DATE (1976)	ORBIT NUMBER	Frame Numbers 4/6	Frame Numbers 5/7	TIME H:M:S	CO-ORDS OF CENTRE LATITUDE	CO-ORDS OF CENTRE LONGITUDE
2359	16 JANUARY	5002	167	183	11:06:30	N51:32	W013:01
"	"	"	199	215			
			168	184	11:07:00	N50:07	W013:42
			200	216			
2378	4 FEBRUARY	5267	028	049	11:09:50	N58:26	W010:29
			070	091			
"	"	"	029	050	11:10:20	N57:02	W011:23
			071	092			
"	"	"	030	051	11:10:40	N55:39	W012:15
			072	093			
"	"	"	031	052	11:11:10	N54:15	W013:03
			073	094			
"	"	"	032	053	11:11:30	N52:51	W013:48
			074	095			
2380	6 FEBRUARY	5295	102	123	11:21:00	N59:41	W012:30
			144	165			
"	"	"	103	124	11:21:20	N58:18	W013:28
			145	166			
2383	9 FEBRUARY	5336	059	079	09:57:40	N49:55	E003:22
			099	119			
"	"	"	060	080	09:58:10	N48:30	E002:43
			100	120			
2384	10 FEBRUARY	5350	072	091	10:02:40	N52:42	E003:17
			110	129			
"	"	"	073	092	10:03:00	N51:18	E002:35
			111	130			
"	"	"	074	093	10:03:30	N49:54	E001:56
			112	131			
"	"	"	075	094	10:03:50	N48:29	E001:18
			113	132			
2385	11 FEBRUARY	5364	092	115	10:07:30	N55:38	E003:30
			138	161			
"	"	"	093	116	10:07:50	N54:15	E002:43
			139	162			
"	"	"	094	117	10:08:20	N52:51	E001:58
			140	163			
"	"	"	095	118	10:08:40	N51:27	E001:15
			141	164			
"	"	"	096	119	10:09:10	N50:03	E000:34
			142	165			
"	"	"	097	120	10:09:30	N48:39	W000:05
			143	166			
2386	12 FEBRUARY	5378	122	156	10:12:20	N58:24	E003:48
			190	224			
"	"	"	123	157	10:12:40	N57:01	E002:54
			191	225			

DAY Since Launch	DATE (1976)	ORBIT NUMBER	Frame Numbers 4/6	Frame Numbers 5/7	TIME H : M : S	CO-ORDS OF CENTRE LATITUDE	CO-ORDS OF CENTRE LONGITUDE
2386	12 FEBRUARY	5378	124	158	10:13:10	N55:37	E002:03
			192	226			
"	"	"	125	159	10:13:30	N54:13	E001:16
			193	227			
"	"	"	126	160	10:14:00	N52:49	E000:31
			194	228			
"	"	"	127	161	10:14:20	N51:25	W000:11
			195	229			
"	"	"	128	162	10:14:50	N50:01	W000:51
			196	230			
"	"	"	MSG	MSG	10:15:10	N48:37	W001:30
			197	231			
2387	13 FEBRUARY	5392	020	042	10:17:40	N59:48	E003:19
			064	086			
"	"	"	021	043	10:18:00	N58:25	E002:22
			065	087			
"	"	"	022	040	10:18:30	N57:02	E001:29
			066	088			
"	"	"	209	MSG	10:18:50	N55:39	E000:38
			MSG	MSG			
"	"	"	210	233	10:19:20	N54:15	W000:09
			256	279			
"	"	"	211	234	10:19:40	N52:51	W000:54
			257	280			
"	"	"	212	235	10:20:10	N51:28	W001:36
			258	281			
"	"	"	213	236	10:20:30	N50:04	W002:16
			259	282			
2388	14 FEBRUARY	5406	078	100	10:23:20	N59:47	E001:54
			122	144			
"	"	"	079	101	10:23:40	N58:24	E000:57
			123	145			
"	"	"	080	102	10:24:10	N57:01	E000:03
			124	146			
"	"	"	081	103	10:24:30	N55:38	W000:47
			125	147			
"	"	"	082	104	10:25:00	N54:14	W001:35
			126	148			
"	"	"	083	105	10:25:20	N52:50	W002:20
			127	149			
"	"	"	084	106	10:25:50	N51:27	W003:03
			128	150			
"	"	"	085	107	10:26:10	N50:03	W003:43
			129	151			
"	"	"	086	108	10:26:40	N48:39	W004:22
			130	152			
2389	15 FEBRUARY	5420	024	053	10:29:00	N59:46	E000:28
			082	111			
"	"	"	025	054	10:29:30	N58:24	W000:30
			083	112			
"	"	"	001	028	10:29:50	N57:01	W001:24
			055	082			

DAY Since Launch	DATE (1976)	ORBIT NUMBER	Frame Numbers 4/6	Frame Numbers 5/7	TIME H:M:S	CO-ORDS OF CENTRE LATITUDE	CO-ORDS OF CENTRE LONGITUDE
2389	15 FEBRUARY	5420	002	029			
			056	083	10:30:20	N55:37	W002:14
"	"	"	003	030			
			057	084	10:30:40	N54:14	W003:02
"	"	"	004	031			
			058	085	10:31:10	N52:50	W003:47
"	"	"	005	032			
			059	086	10:31:30	N51:26	W004:30
"	"	"	006	033			
			060	087	10:32:00	N50:02	W005:10
"	"	"	007	034			
			061	088	10:32:20	N48:38	W005:49
2391	17 FEBRUARY	5448	001	022			
			043	064	10:40:30	N59:45	W002:23
"	"	"	002	023			
			044	065	10:40:50	N58:23	W003:21
"	"	"	277	MSG			
			MSG	MSG	10:41:20	N57:00	W004:14
"	"	"	278	299			
			320	341	10:41:40	N55:36	W005:05
"	"	"	279	300			
			321	342	10:42:10	N54:13	W005:52
"	"	"	280	301			
			322	343	10:42:30	N52:49	W006:37
"	"	"	281	302			
			323	344	10:43:00	N51:25	W007:19
"	"	"	282	303			
			324	345	10:43:20	N50:00	W007:59
"	"	"	283	304			
			325	346	10:43:50	N48:36	W008:38
2392	18 FEBRUARY	5462	014	035			
			056	077	10:46:10	N59 50	W003:49
"	"	"	015	036			
			057	078	10:46:30	N58:28	W004:47
"	"	"	016	037			
			058	079	10:47:00	N57:06	W005 40
"	"	"	017	038			
			059	080	10:47:20	N55 42	W006:30
"	"	"	018	039			
			060	081	10:47:50	N54:18	W007:17
"	"	"	019	040			
			061	082	10:48:10	N52:54	W008:02
"	"	"	020	041			
			062	083	10:48:40	N51:30	W008:45
"	"	"	001	031			
			MSG	MSG	10:49:30	N48:42	W010:04
2393	19 FEBRUARY	5476	001	023			
			045	067	10:51:50	N59:50	W005:15
"	"	"	002	024			
			046	068	10:52:20	N58:28	W006:12
"	"	"	003	025			
			047	069	10:52:40	N57:04	W007:06

DAY Since Launch	DATE (1976)	ORBIT NUMBER	Frame Numbers 4 6	Frame Numbers 5 7	TIME H : M : S	CO-ORDS OF CENTRE LATITUDE	CO-ORDS OF CENTRE LONGITUDE
			004	026			
2393	19 FEBRUARY	5476	047	070	10:53:10	N55:41	W007:57
			005	027			
"	"	"	048	071	10:53:30	N54:17	W008:44
			006	028			
"	"	"	049	072	10:54:00	N52:52	W009:28
			007	029			
"	"	"	050	073	10:54:20	N51:29	W010:10
			008	030			
"	"	"	051	074	10:54:50	N50:05	W010:51
			009	031			
"	"	"	052	075	10:55:10	N48:40	W011:29
			288	308			
2394	20 FEBRUARY	5490	328	348	10:57:40	N59:50	W006:39
			289	309			
"	"	"	329	349	10:58:00	N58:27	W007:37
			290	310			
"	"	"	330	350	10:58:30	N57:04	W008:32
			291	311			
"	"	"	331	351	10:58:50	N55:41	W009:23
			292	312			
"	"	"	332	352	10:59:20	N54:17	W010:11
			293	313			
"	"	"	333	353	10:59:40	N52:53	W010:56
			294	314			
"	"	"	334	354	11:00:10	N51:29	W011:39
			295	315			
"	"	"	335	355	11:00:30	N50:05	W012:19
			296	316			
"	"	"	336	356	11:01:00	N48:41	W012:57
			015	040			
2395	21 FEBRUARY	5504	065	090	11:03:20	N59:51	W008:05
			016	041			
"	"	"	066	091	11:03:40	N58:29	W009:03
			017	042			
"	"	"	067	092	11:04:10	N57:07	W009:57
			018	043			
"	"	"	068	093	11:04:30	N55:43	W010:48
			019	044			
"	"	"	069	094	11:05:00	N54:19	W011:35
			020	045			
"	"	"	070	095	11:05:20	N52:56	W012:20
			021	046			
"	"	"	071	096	11:05:50	N51:32	W013:03
			022	047			
"	"	"	072	097	11:06:10	N58:08	W013:43
			008	026			
2401	27 FEBRUARY	5587	044	062	09:57:10	N50:07	E003:28
			009	027			
"	"	"	045	063	09:57:40	N48:42	E002:50

DAY Since Launch	DATE (1976)	ORBIT NUMBER	Frame Numbers 4/6	Frame Numbers 5/7	TIME H : M : S	Co-ords of Centre LATITUDE	Co-ords of Centre LONGITUDE
			015	036			
2402	28 FEBRUARY	5601	057	078	10:02:10	N52:54	E003·24
			016	037			
"	"	"	058	079	10:02:30	N51:30	E002·42
			018	039			
"	"	"	060	081	10:03:20	N48:42	E001:23
			005	018			
2403	29 FEBRUARY	5615	031	044	10:07:00	N55:43	E003:30
			006	019			
"	"	"	032	045	10:07:20	N54:20	E002:43
			007	020			
"	"	"	033	046	10:07:50	N52:56	E001:58
			008	021			
"	"	"	034	047	10:08:10	N51:32	E001:16
			009	022			
"	"	"	035	048	10:08:40	N50:08	E000:36
			010	023			
"	"	"	036	049	10:09:00	N48:43	W000:02
			012	040			
2422	19 MARCH	5880	068	096	10:13:00	N53:00	E000:36
			013	041			
"	"	"	069	097	10:13:20	N51:36	W000:06
			014	042			
"	"	"	070	098	10:13:50	N50:13	W000:47
			MSG	027			
2423	20 MARCH	5894	051	075	10:19:30	N50:14	W002:11
			003	017			
2424	21 MARCH	5908	031	045	10:24:50	N51:35	W002:58
			004	018			
"	"	"	032	046	10:25:10	N50:11	W003:38
			005	019			
"	"	"	033	047	10:25:40	N48:47	W004:17
			168	202			
2425	22 MARCH	5922	236	270	10:29:10	N55:48	W002:10
			169	203			
"	"	"	237	271	10:29:40	N54:25	W002:57
			170	204			
"	"	"	238	272	10:30:00	N53:01	W003:42
			171	205			
"	"	"	239	273	10:30:30	N51:37	W004:25
			172	206			
"	"	"	240	274	10:30:50	N50:13	W005:05
			173	207			
"	"	"	241	275	10:31:20	N48:48	W005:43
2426	23 MARCH	5936	078	100	10:34:30	N57:14	W002:43
			122	144			
2427	24 MARCH	5950	012	036	10:39:50	N58:39	W003:15
			MSG	084			

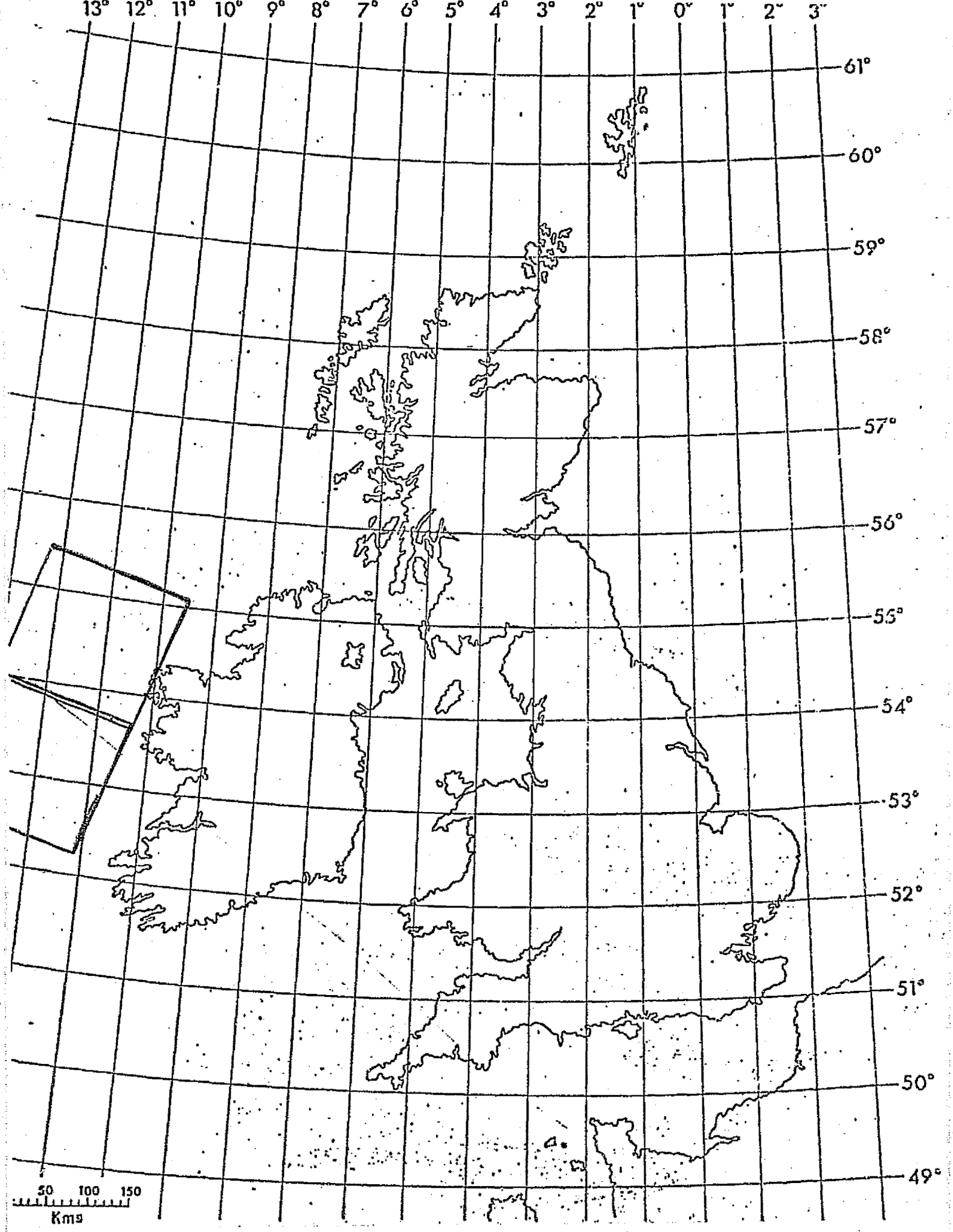

Fig. 1(a): Landsat coverage of the British Isles, Cycle 17, 29th November - 16th December, 1975.

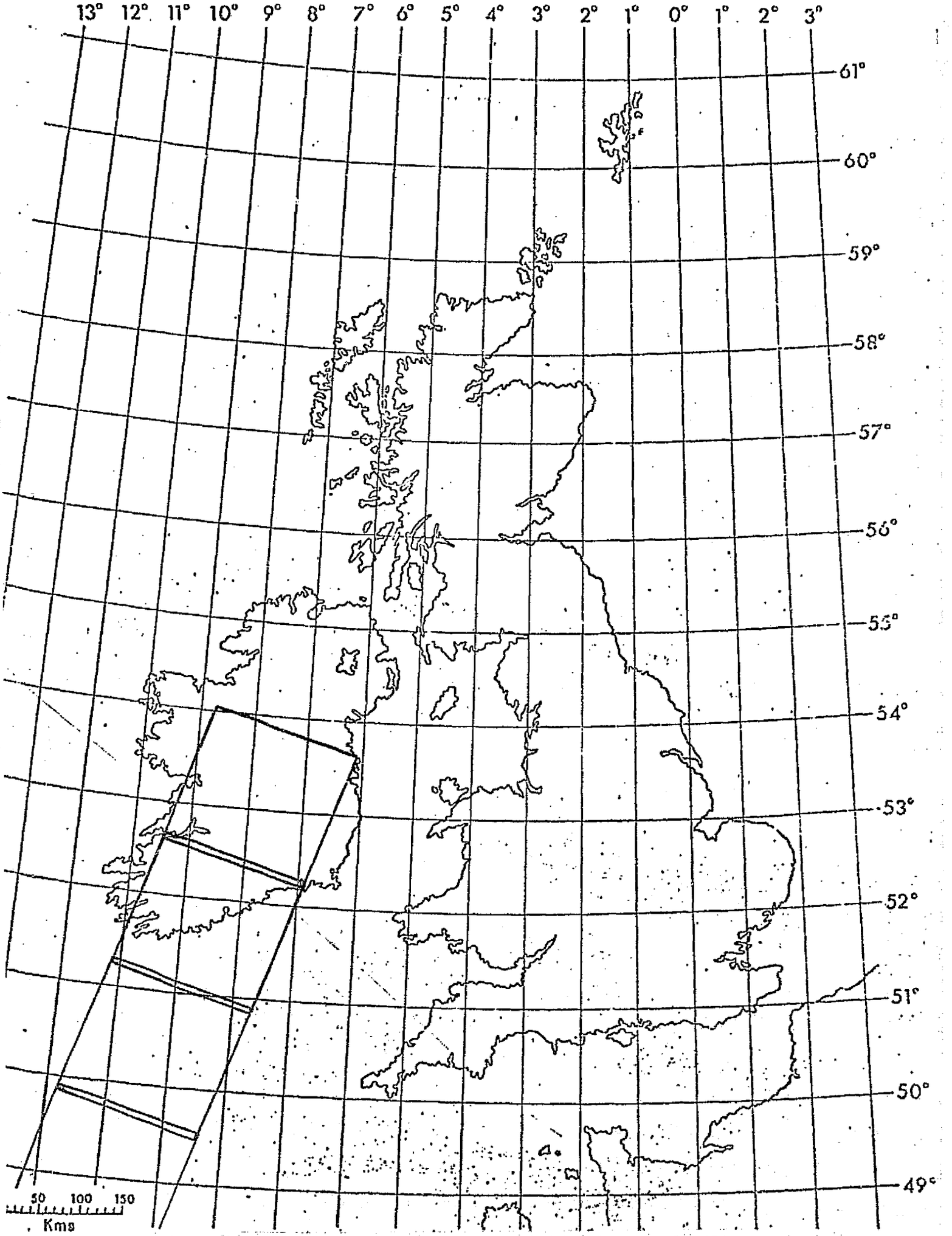

Fig. 1(b): Landsat coverage of the British Isles, Cycle 18, 17th December, 1975 - 3rd January, 1976.

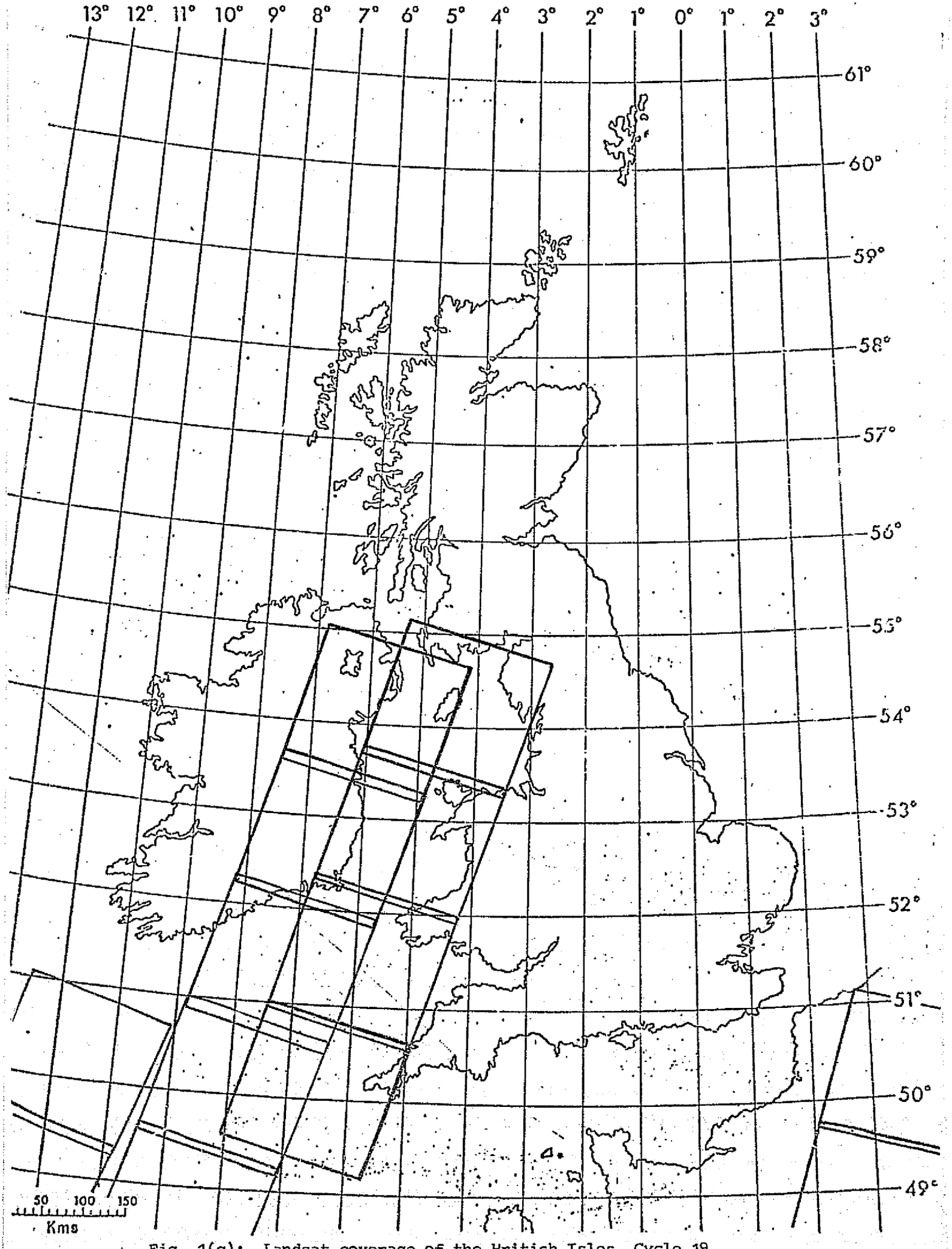

Fig. 1(c): Landsat coverage of the British Isles, Cycle 19, 4th January, 1976 – 21st January, 1976.

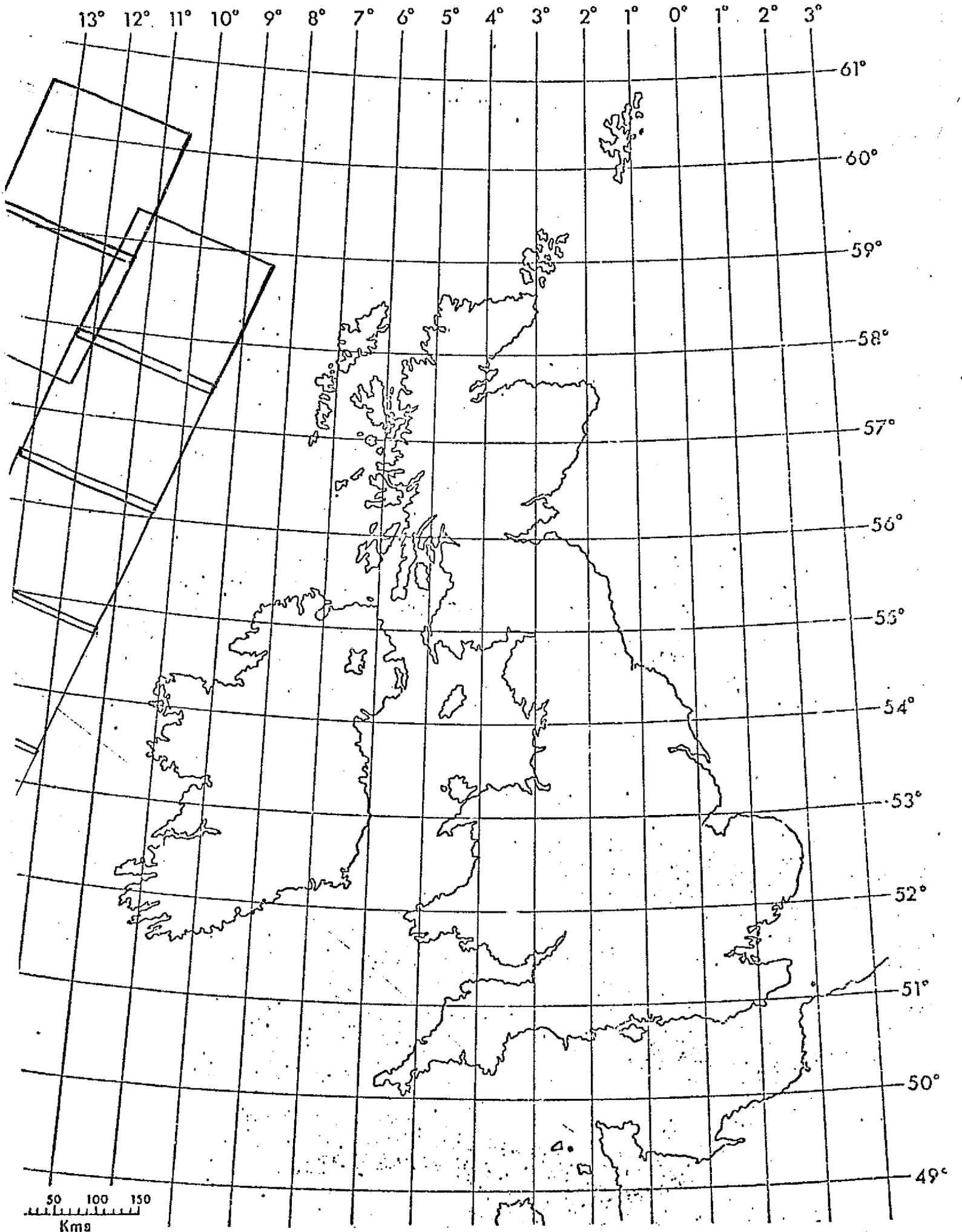

Fig. 1(d): Landsat coverage of the British Isles, Cycle 20, 22nd January - 8th February, 1976.

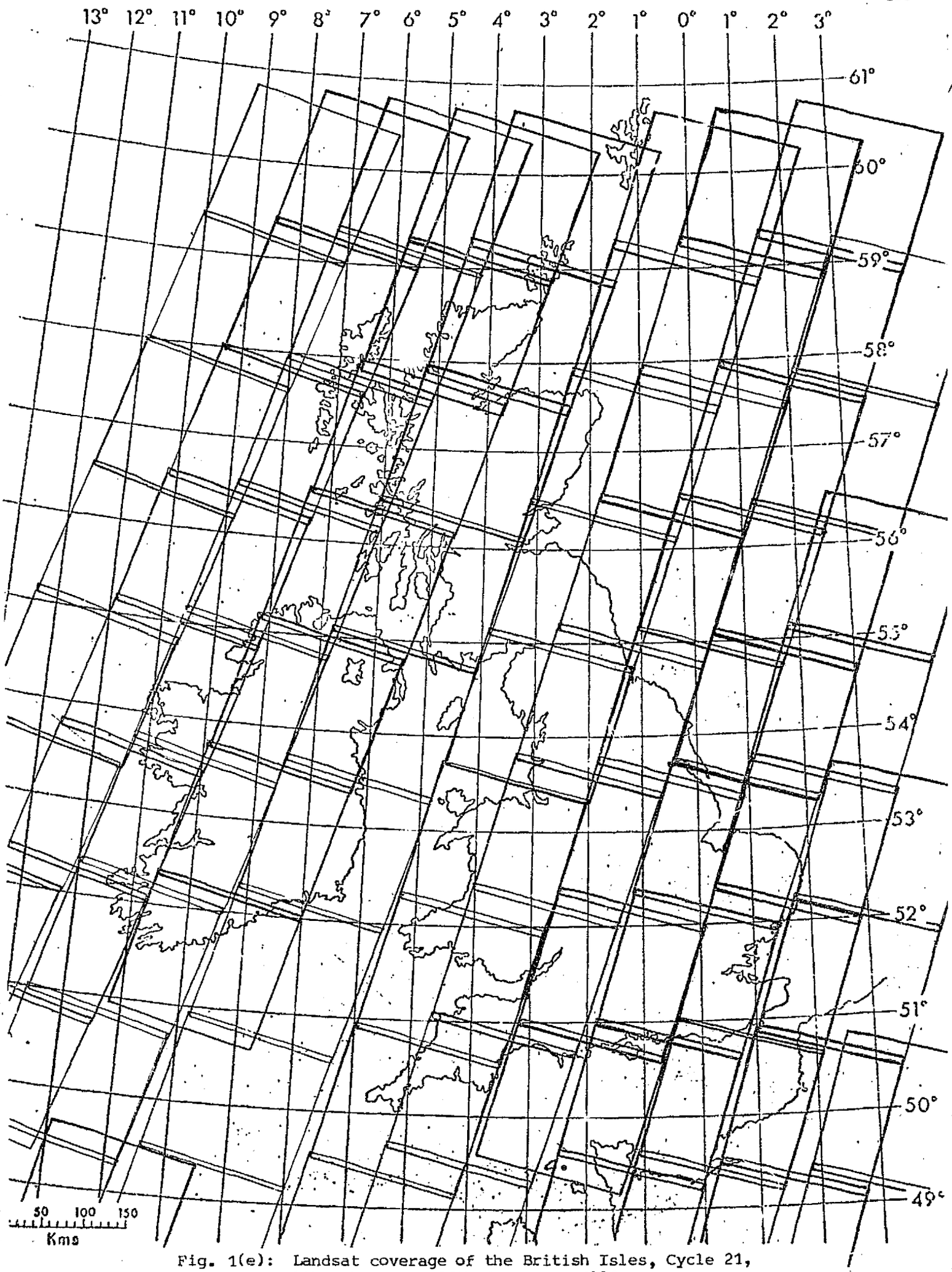

Fig. 1(e): Landsat coverage of the British Isles, Cycle 21, 9th February - 26th February, 1976.

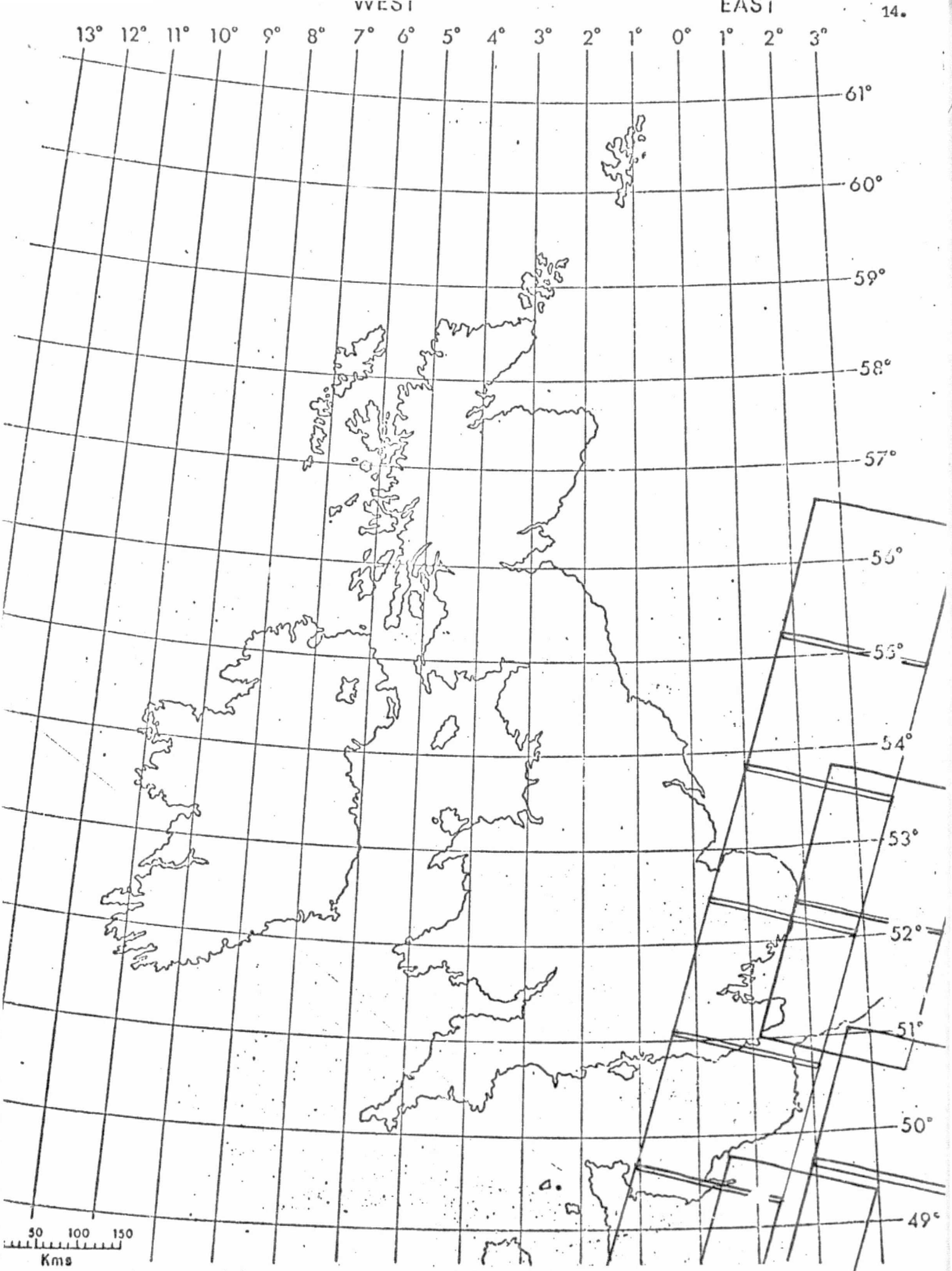

Fig. 1(f): Landsat coverage of the British Isles, Cycle 22, 27th February - 15th March, 1976.

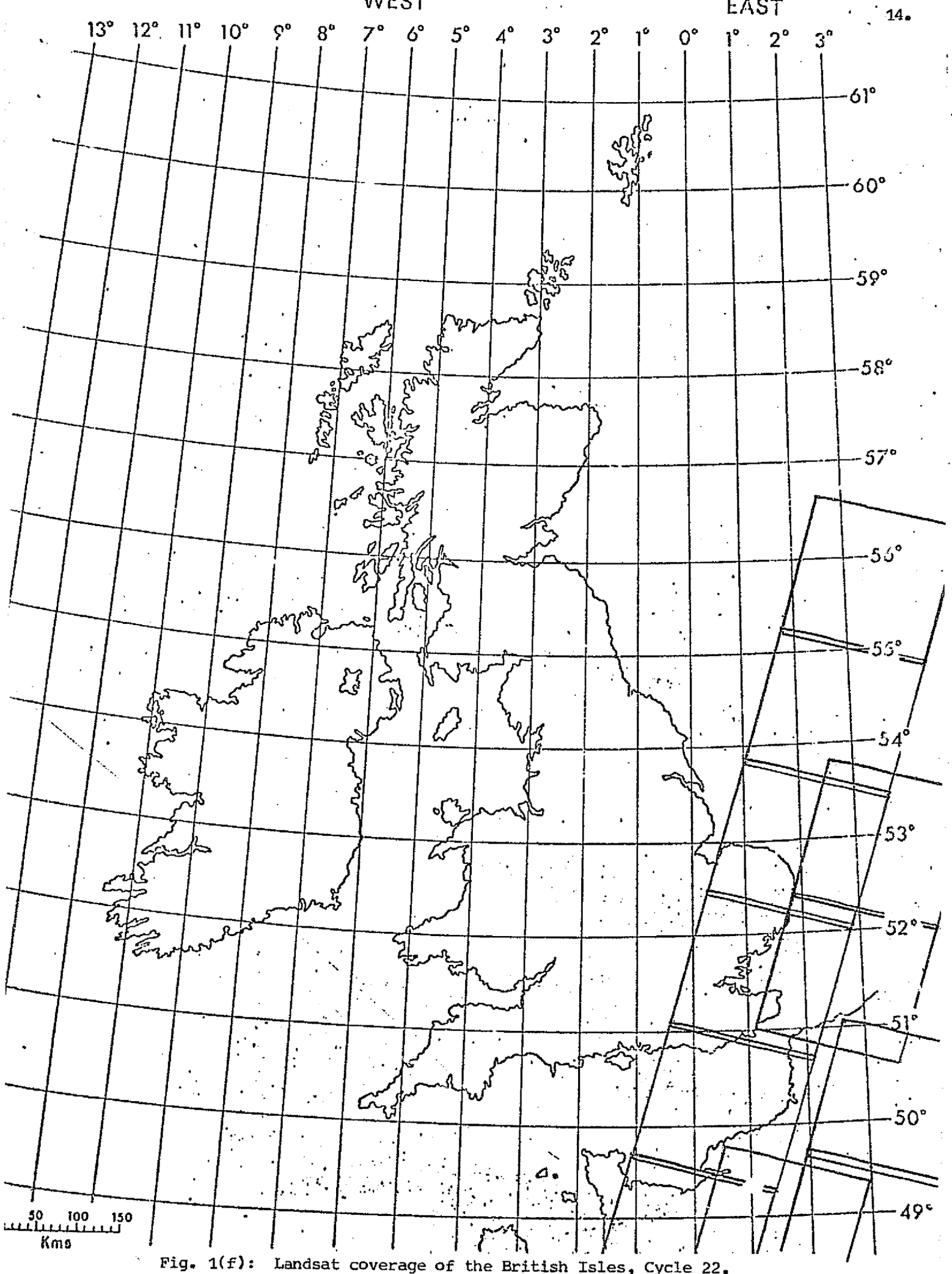

Fig. 1(f): Landsat coverage of the British Isles, Cycle 22, 27th February - 15th March, 1976.

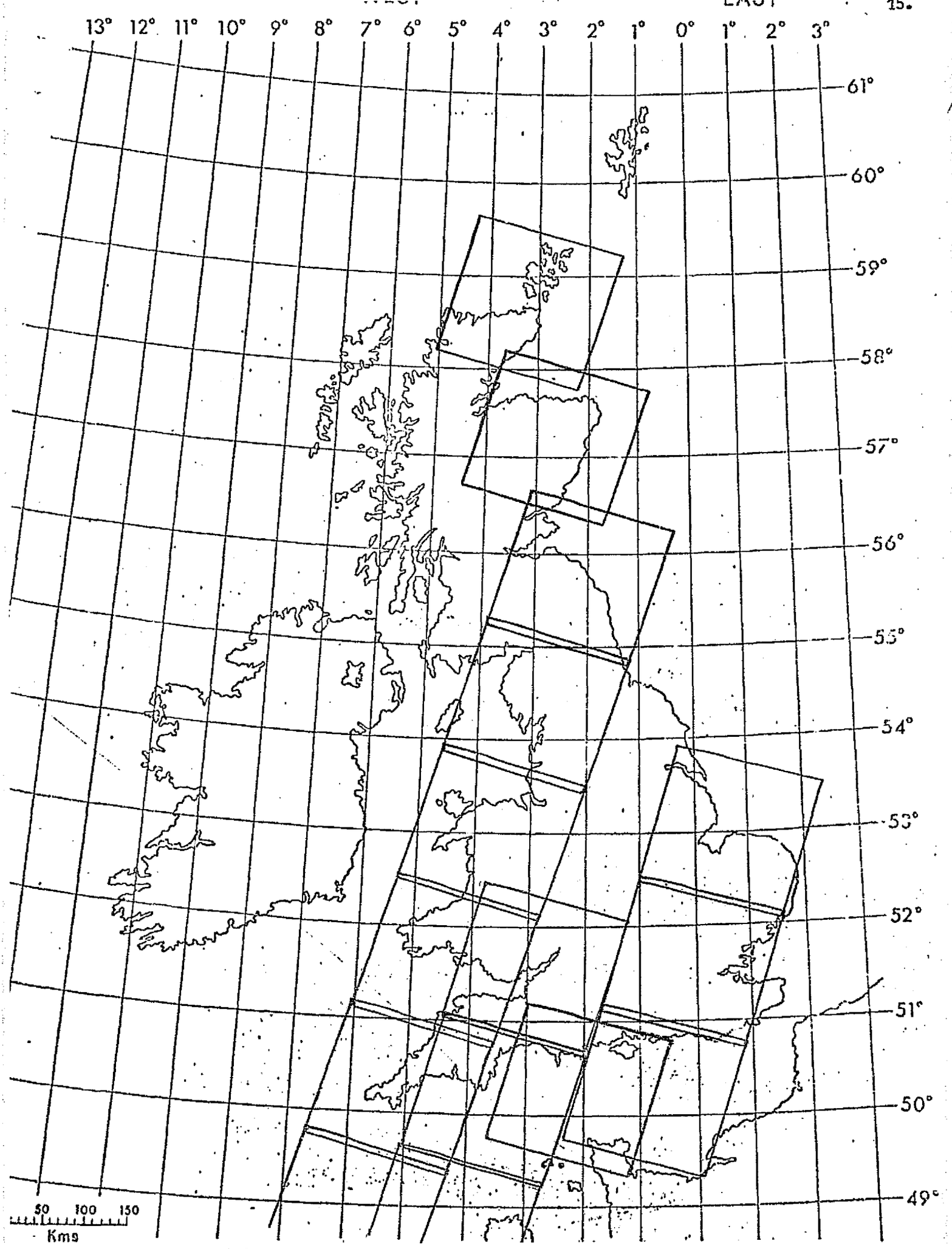

Fig. 1(g): Landsat coverage of the British Isles, Cycle 23, 16th March - 2nd April, 1976.

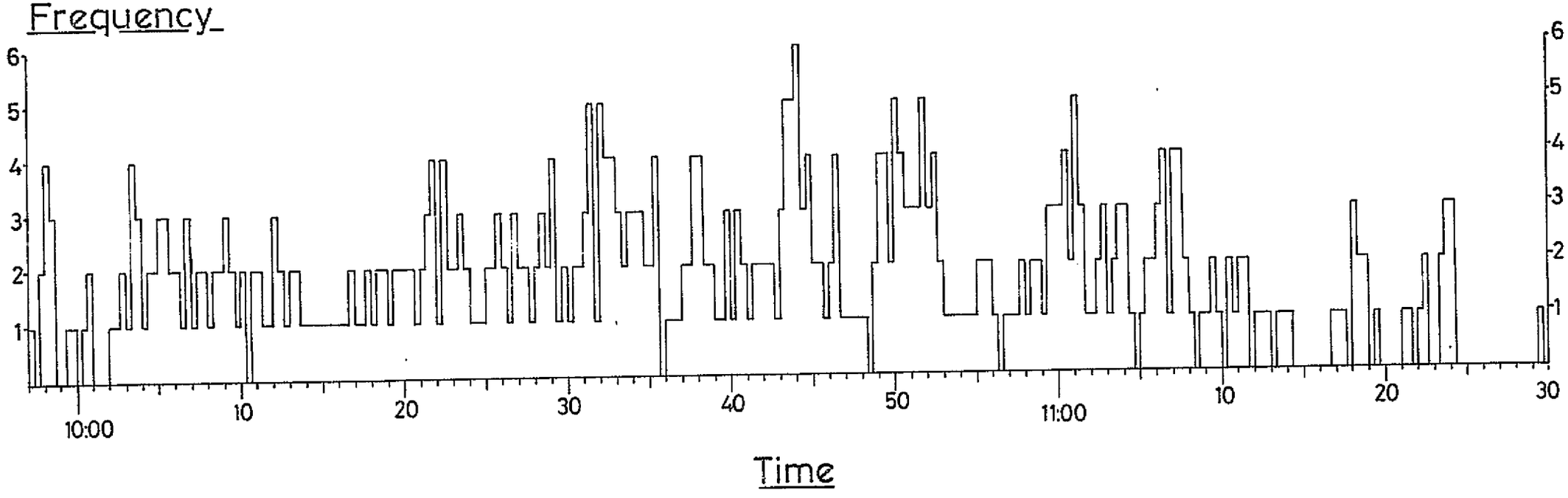

Fig. 2: Distribution of the imagery through time.

Indeed, there seems to have been a widely-accepted belief that Landsat imagery is ill-suited to cloud studies because cloudiness is thought to saturate the pictures easily (see, e.g. Danko, ibid.).
Dependent as we have been on image data, not CCTs, we are not in a position to comment conclusively on this belief: there are more uncertainties in the analysis of Landsat images than CCTs, stemming mostly from picture processing. Taking as many of these uncertainties into account as we are readily able to do, and working at something less than the nominal full resolution of the Landsat images, it appears that the principal families of clouds do possess distinctive spectral signatures, and yield different histograms of picture brightness over mesoscale areas of cloud fields.

The implications of these findings are discussed in relation to other work in this Department concerned with automatic (objective) analyses of cloud imagery from meteorological satellites. The biggest potential advantage that an automatic multispectral cloud mapping methodology might enjoy over one based on single waveband data seems to be that that might be able to utilise the full spatial resolution of the original observations, rather than the reduced resolution which results from most methods of texture analysis.

The choice of sampling area was important in view of the characteristics of the cloud fields we wished to investigate, the imagery we chose to use in our analyses, and the capabilities of the equipment available for the task:

a) Cloud field characteristics. Although it would have been possible to select a brightness threshold to represent the edge of the cloud portrayed in any image so that non-cloud areas might have been excluded from the study, we did not think it necessary or indeed desirable to take such a step. We did not want to make initial assumptions which might influence the

shapes of image brightness/frequency distributions, especially since the characteristics of cloud margins, and the spaces between adjacent structural elements of cloud fields might significantly assist in some aspects of the automatic recognition of different families of clouds.

b) The form of the imagery. In view of the added problems that would have been associated with copying and enlarging the 70 mm transparencies provided by NASA, we decided to analyse these images themselves. At this scale 1 mm represents approximately 3.37 km on the ground.

c) The microdensitometer. The instrument we used was a System P-1000 Photoscan, manufactured by Optronics International Inc. This is a high-speed digital microdensitometer. The machine incorporates an electro-optical rotating drum which converts photometric data on film negatives or positives to digital form for computer processing. In order that an image may be scanned it is placed over an opening in the drum, and clamped to it so that the film adheres exactly to its machined cylindrical surface dimensions.

In the present study a sampling area of 10 mm^2 was chosen. We wished to sample a sufficiently large area to establish whether the brightness characteristics of fields of different categories of cloud are indeed as clear as eyeball investigations seem to suggest. It seemed likely that cloud fields should be distinguishable from one another if viewed sufficiently broadly to account for their textural characteristics; whether cloud families could be differentiated on the basis of their reflectance characteristics per unit area seemed to be more doubtful. Our hope was that, by compiling sufficiently large populations of summary statistics for quite large areas, both issues might be elucidated simultaneously, the first through areal brightness/frequency distributions, the second through the spectral reflectance graphs constructed for each

cloud category from the results for the modal classes in each brightness/frequency histogram.

Accurate registration was attempted for each set of imagery using a clean perspex mask on which were placed the locations of the four registration marks of each frame. In this way the four images of each cloud scene could be registered and a common sampling area identified.

II TECHNIQUES

1. Selection of imagery

It was established earlier in this project that major cloud types can be differentiated and identified with confidence in Landsat imagery. The cloud families recognised thus were cumulonimbiform, cumuliform, stratiform, stratocumuliform and cirriform. Certain Landsat images were selected to represent "classic" forms of these cloud families and their chief members or cloud types. (See Barrett and Grant, 1976(a), especially Plates 1-5). For our multispectral study we chose one example of each cloud family, plus an example of the cumulocongestus cloud type, the latter on the grounds that cumulus humilis or mediocris and cumulocongestus have substantially different appearances in the Landsat images. Since all four spectral bands were to be investigated, there was a set of 24 cloud images to be analysed.

All 24 images depicted sea areas around the British Isles. Background brightness constitutes a serious problem for any programme of automatic analysis of cloud imagery. Methods have been devised to solve this problem (see, e.g. Miller, 1971), but none have been (or could be?) entirely satisfactory. We wished to reduce, rather than solve, the problem by analysing clouds viewed-over surfaces with relatively even and constant brightness responses. Sea surfaces meet these conditions much better than land surfaces, especially in the British region, where convergences of major currents do not occur.

2. Selection of sampling area

This was defined on the mask by straight-edged, machine-cut, metal foil strips which overlapped to provide a precisely measured imaging area. In operation each image was orientated correctly on the mask provided for its cloud category, and the image with its mask were then located on the imaging drum.

The Koehler illumination system of the Photoscan ensures uniform illumination and focussing on the film surface via turret mounted apertures. The light transmitted through each image is measured using a photo-detector, and converted to 256 grey-levels.

The choice of scanning aperture is important, as this determines the sampling size for the imagery. The aperture sizes available for imaging on the Bristol University machine are threefold, namely 25, 50 or 100 μm square. In the NASA Landsat Data Users Handbook (1971) (see H 1.4, "Photographic Micro-Image Quality') the following is found:

> "Because of MTF, granularity, and sensor and recording systems considerations, scans using apertures smaller than ~ 20 μm diameter will be essentially meaningless. Even scans with aperture sizes of ~ 40 μm will probably not correlate well with macro-density readings even when assuming that the investigator has made necessary corrections from specular to diffuse density"

With such considerations in mind, the largest imaging aperture size available (100 μm) was selected in order to minimise the sources of error. An aperture of 100 μm square corresponds on the image to an area of approximately 337 metres square on the ground. Thus approximately 16 pixels were analysed in each of our microdensitometer spot readings.

3. Operating practices

The illuminating and imaging optics of the Photoscan are mounted on opposite sides of a "C" carriage through which the cylinder drum rotates.

The optical density of each image is measured every 100 μm along the circumference of the drum (Y direction) within the pre-determined area. After each revolution the "C" carriage is stepped in the axial (X) direction by 100 μm. In practice these processes were repeated until the whole 10 mm^2 area of each image had been scanned. Once per revolution, through an opening in the drum opposite the film position, the densitometer photo-detector system is reset to a given known value which represents an optical density of zero as defined by the air path through the slot. Since the drum speed is high (8 revs. per second) the drift of the instrument is far less significant than the least significant bit of density data.

The detector voltage resulting from light transmitted through each image is amplified logarithmically, digitized, displayed, and recorded by interfacing the scanner with a magnetic tape recorder. Each number is representative of a grey-level in the selected density range. In our case the density range was 0 to 2D. Within this range density bears a linear relationship with the output grey levels.

Optical density (D) is defined as:

$$D = \log \frac{Ii}{It}$$

where

Ii is the light intensity impinging on the detector through an air path and

It is the light intensity of the transmitted light.

In addition to the 10 mm^2 sampling area on each image, the 15 step grey-scale tablet was scanned. This scale has undergone the same copying and processing as the image to which it is attached (NASA, 1971, pages 3-5).

4. Data output

Output from the microdensitometer was recorded on a magnetic tape unit for subsequent processing on a PDP 11/45 mini-computer.

Initial processing was concerned with the recording brightness values of the 15-step grey-scale tablet of each image. A number of data records were examined for each image and the upper boundary value of each of the 15 steps was determined by inspection of the computer print-out. Preferably some type of edge-detection logic (e.g. Rosenfeld, 1970) should have been employed, but this time did not permit. Once the upper boundaries of each step had been determined these values were fed back into the computer in order that the frequency distribution of brightness values for each image could be determined. This procedure was adopted so that we might be able to relate different frequency classes to actual tones on each Landsat image, rather than some arbitrarily chosen density value which might be inappropriate in view of the apparent variations in image processing.

Besides the frequency distributions of the brightness values, other summary statistics were computed also, including means, standard deviations, skewness and kurtosis.

The mean brightness value for each image was determined in the following manner. The store size of the computer is limited (24 k) and was not large enough to hold all the values of each image (8000-9000). Thus the mean brightness value of each record (Y-axis scan) was calculated and the final mean was taken as the mean of the record means. The Standard Deviation was calculated using the final mean derived as outline above. Skewness and kurtosis values were not found directly on the PDP 11/45 because of problems with the computer program. These were calculated from the frequency distributions using a Hewlett Packard 9801A calculator and an appropriate library program (Prog. 1-3).

III RESULTS

1. Brightness characteristics of Landsat positive transparencies

For analytical purposes, all the brightness values produced by the microdensitometer in terms of 256 grey-levels were converted to optical density values in the range 0 to 2D. This was a straight-forward procedure as the density bears a linear relationship with the grey-levels, as noted previously.

Fig. 3 shows the 15-step grey-scale tablets, plotted as a function of density and waveband. The divisions correspond to the upper limit of each step, the procedure for determining which was outlined above. Step 8 of each wedge is shaded to act as a reference. Step 1 (white) is at the left-hand side, and step 15 (black) is at the right-hand side.

Perhaps the most important fact emerging from this diagram is the wide variation of step width. Generally, the brighter steps, with densities less than 1D, are narrower than the darker steps with densities greater than 1D. The first step is somewhat anomalous in that it has no lower limit. Another notable feature is the variation from image to image in position of similar steps. This variation occurs both between wavebands for a particular frame, and also between one frame and another. Thus, for example, in the illustration of cumulus humilis, corresponding steps of band 7 are generally brighter than those of band 6. Such differences are due in part to variations in the processing of Landsat images.

A serious problem of interpretation therefore arises. Are the differences in brightness in a particular scene in different wavebands due principally to differences in target reflectance, or differences in processing? It is clear from our results that the influences of image processing must be borne in mind constantly as we move towards drawing conclusions from these data. Ideally, the two components of variation should be determined and separated; this we could not achieve in our study.

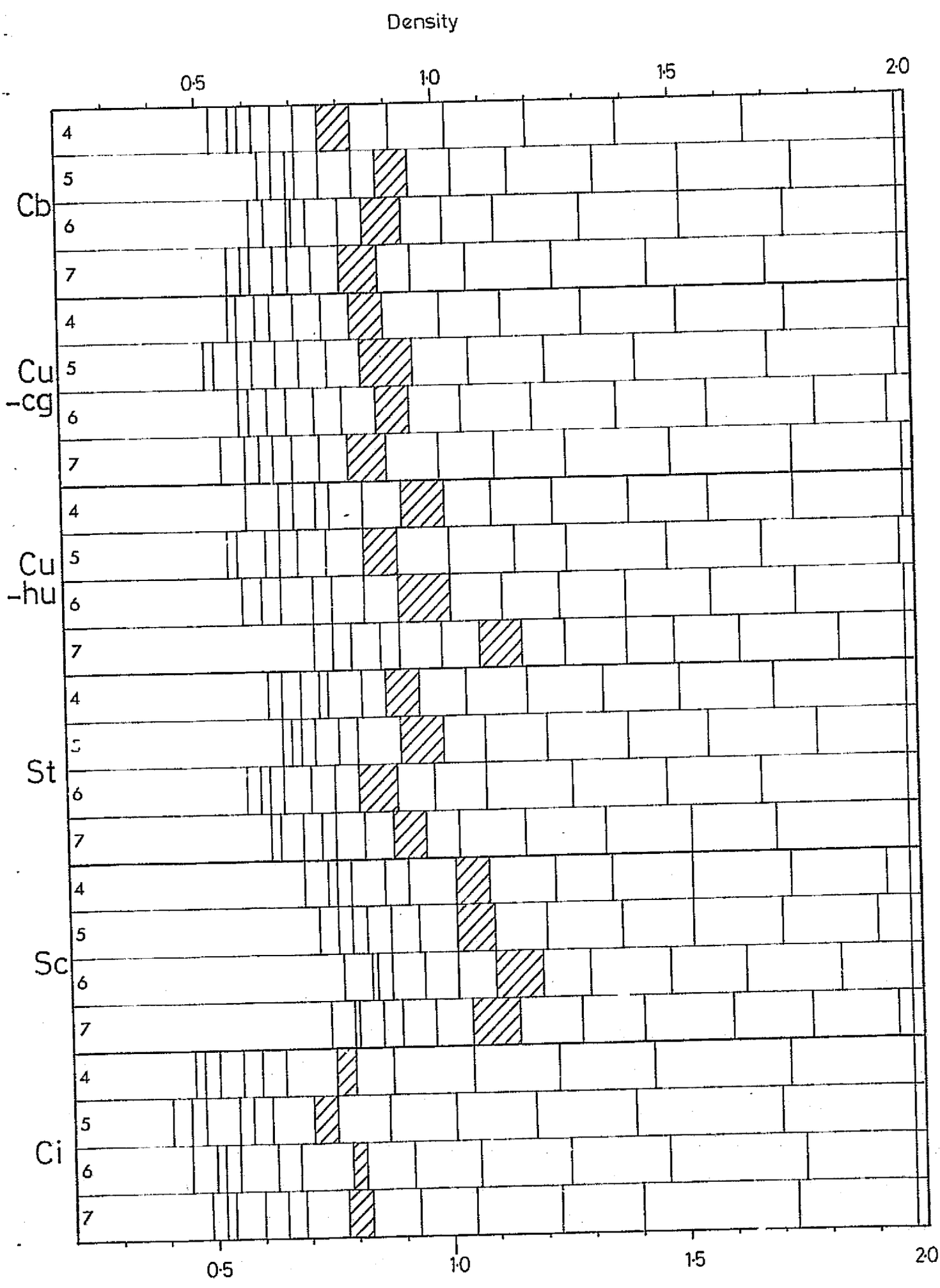

Fig. 3: Grey-Scale Tablets.

2. Brightness characteristics of six categories of clouds: graphical results

Figs. 4 a to f show frequency distributions of individual cloud types in each waveband in relation to the 15 step grey-scale. Frequencies have been converted from number counts to percentages to facilitate comparison between different cloud types. Notwithstanding our earlier comments on variations in picture processing, some important differences do occur.

a) Cumulonimbiform (Fig. 4(a)): Bands 4 and 7 show apparently similar distributions, with band 7 being displaced slightly towards the darker end of the scale. Bands 5 and 6, however, possess a strong modal category, well displaced towards the brighter end of the scale.

b) Cumulus congestus (Fig. 4(b)): The frequency distributions of all four wavebands range across the whole step-wedge scale. All the distributions are essentially similar, some minor differences, occurring at the dark end of the scale in steps 14 and 15.

c) Cumulus humilis (Fig. 4 (c)): Unlike the cumulus congestus graphs of Fig. 4(b), these distributions are restricted in range to the darker end of the scale. This reflects the lower brightness responses of these small cloud cells and the larger areas of dark sea background between them.

d) Stratiform (Fig. 4(d)): Each waveband shows a marked clustering of values at the bright end of the scale, indeed in band 5 almost 100% of the data points are contained within the brightest step. This is undoubtedly due to extensive saturation of the image by this cloud type. The distributions of bands 6 and 7 show tails extending well into the darker portion of the scale.

e) Stratocumuliform (Fig. 4(e)): Bands 4 and 5 have similar distributions, extending across a wide range of values, peaking

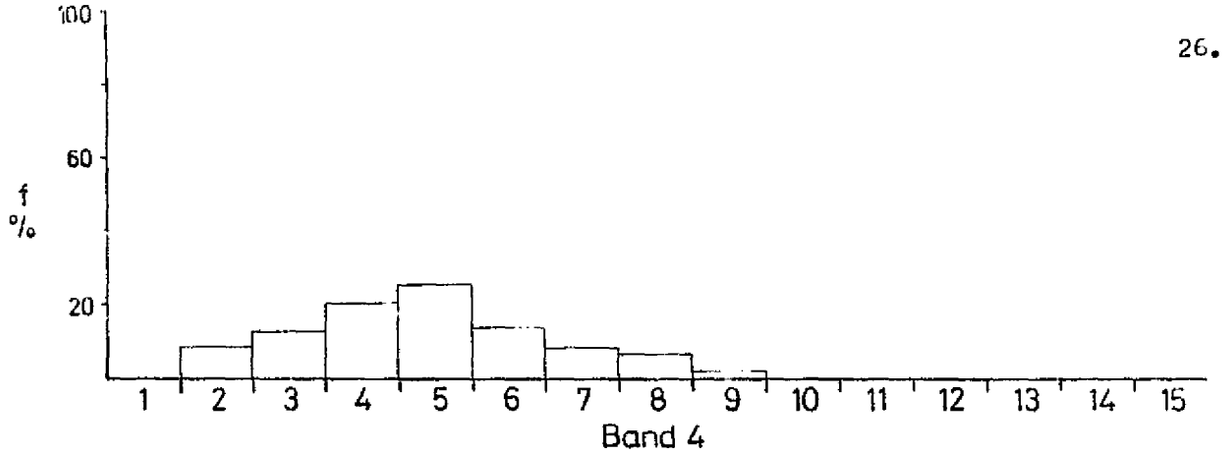

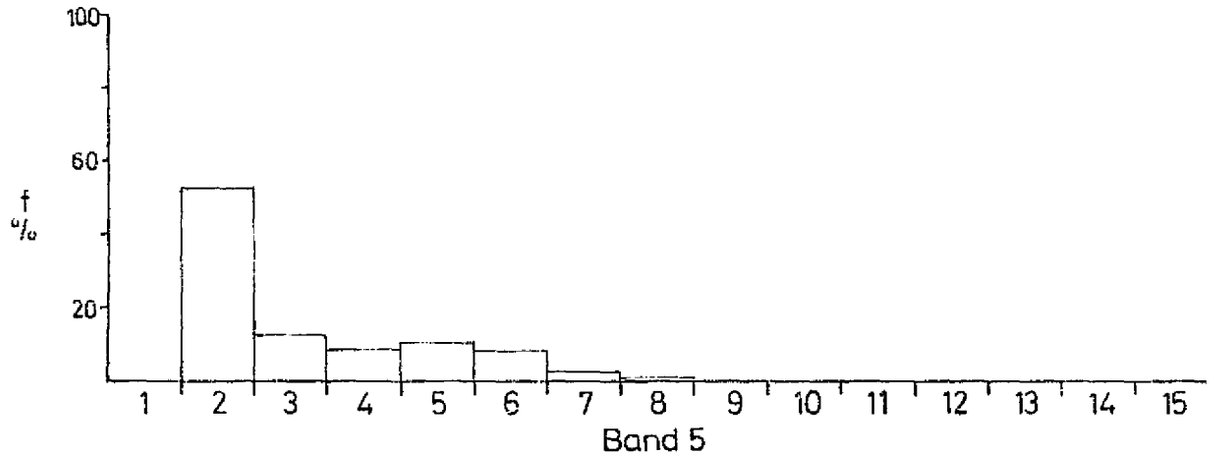

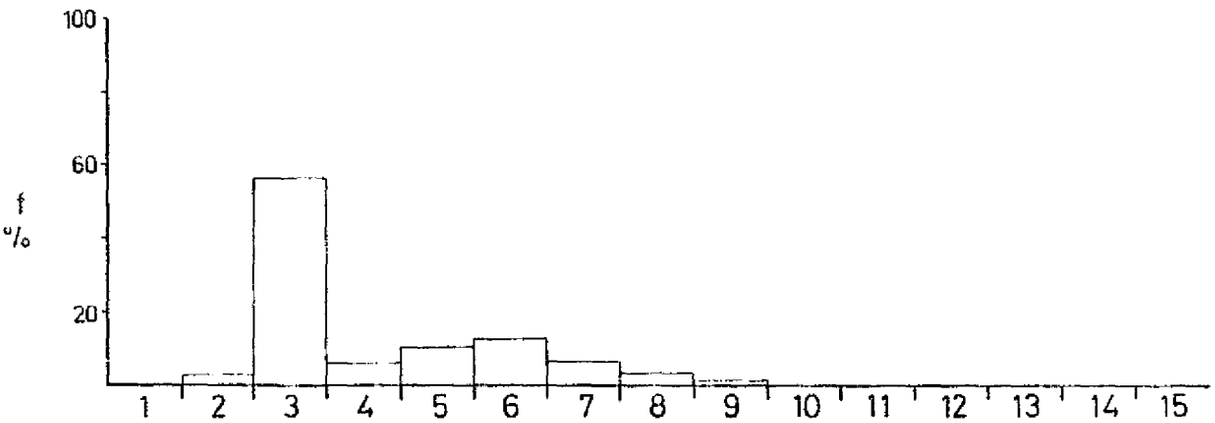

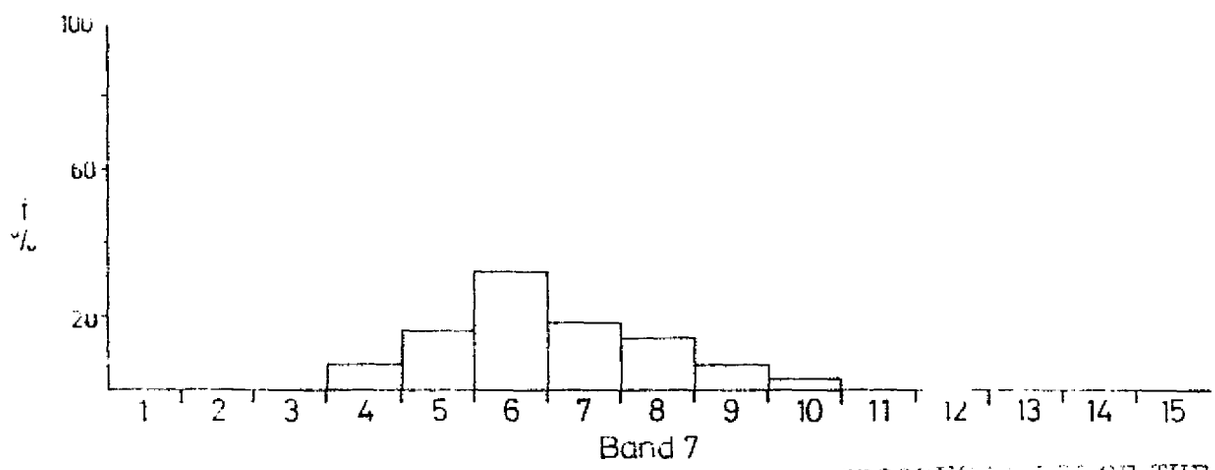

NB Values <1% not shown

Fig. 4(a): Cumulonimbiform: Frequency Distribution.

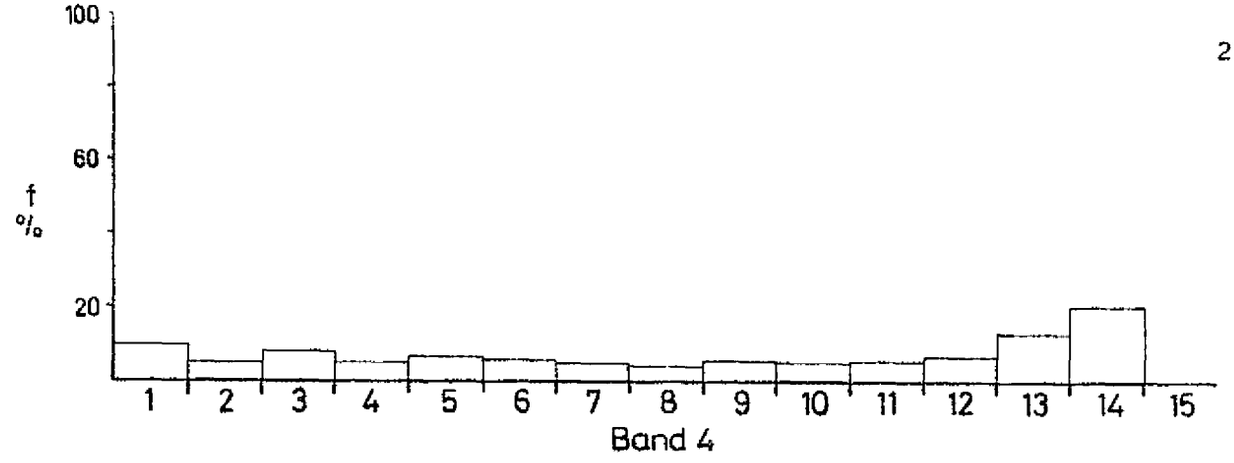

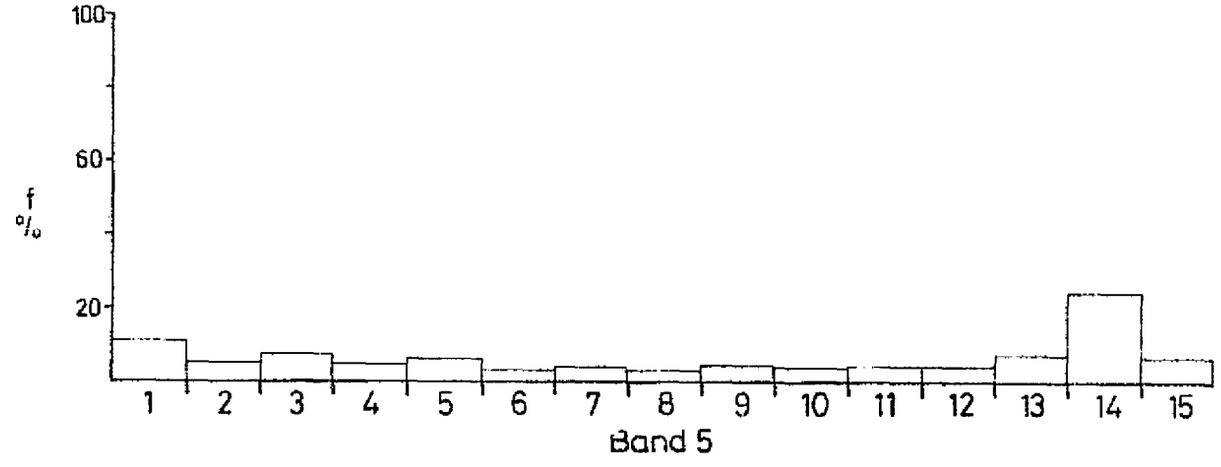

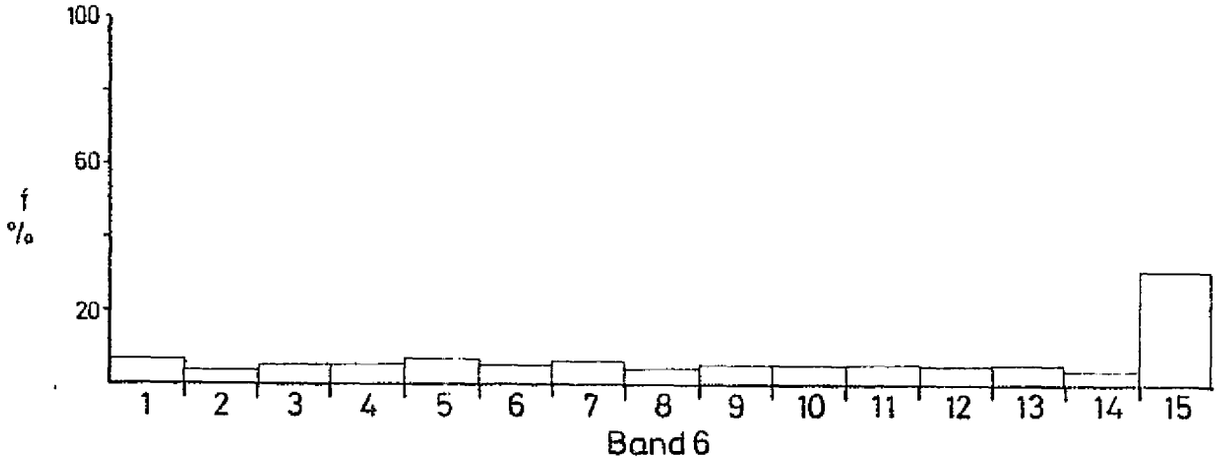

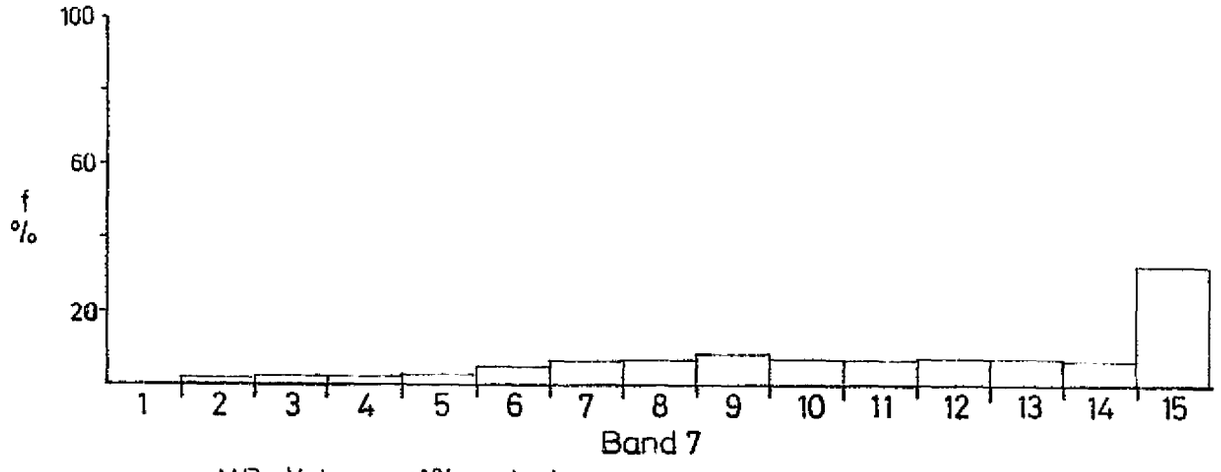

N.B. Values <1% not shown

Fig. 4(b): Cumulus congestus: Frequency Distribution.

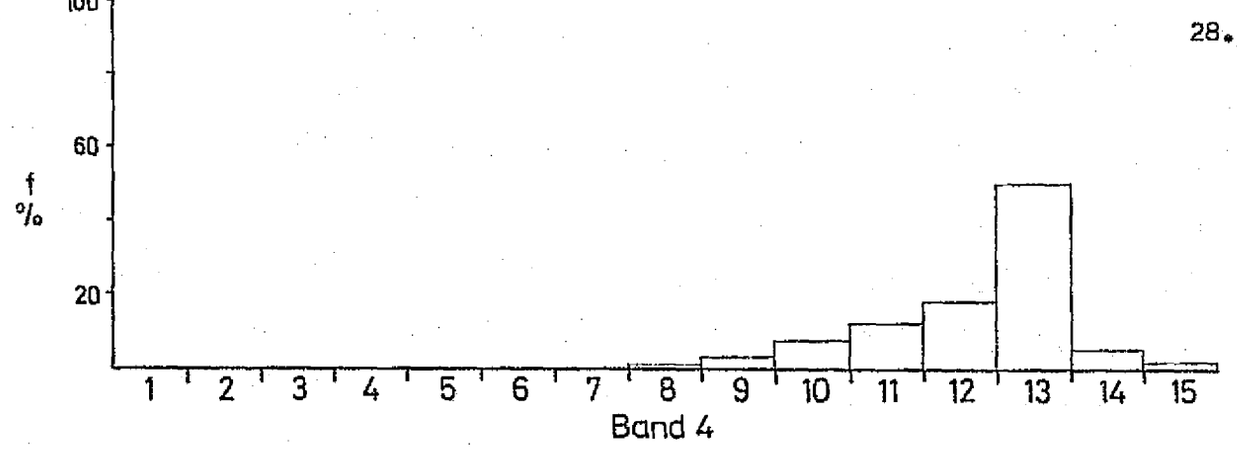

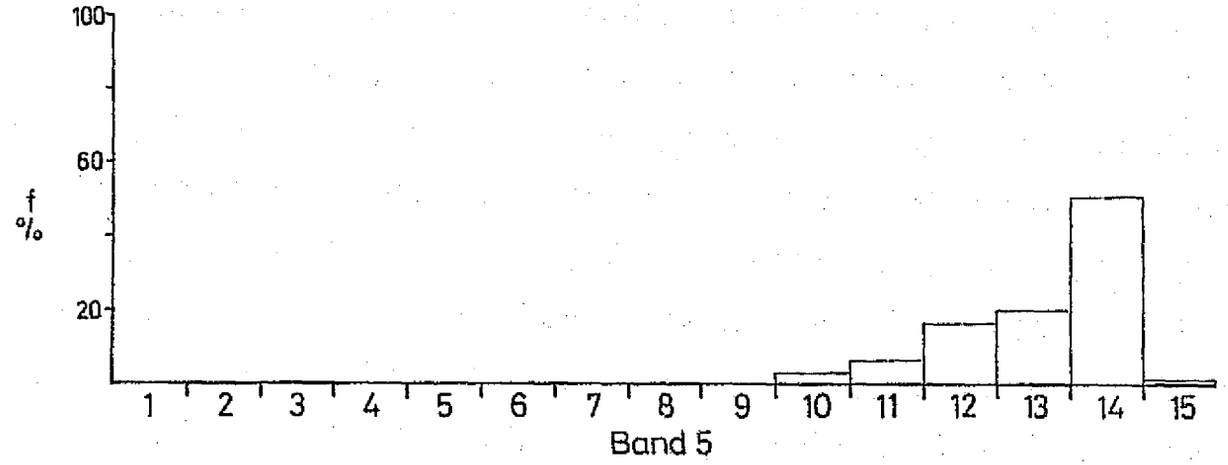

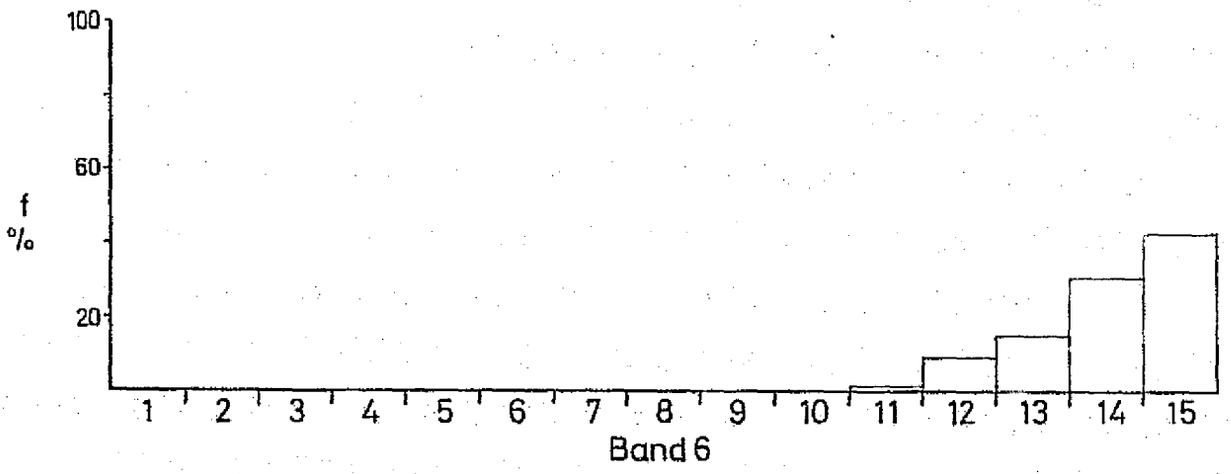

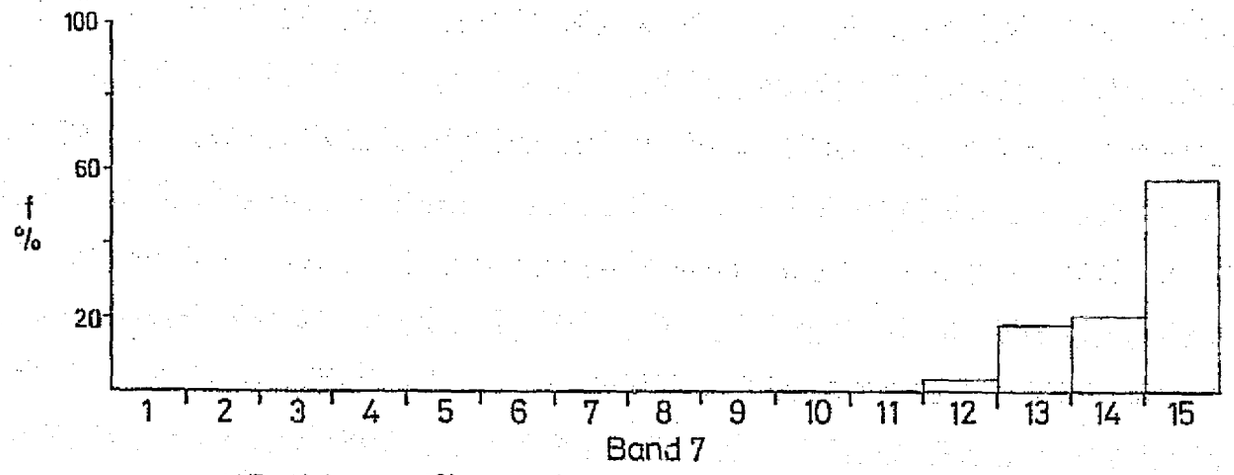

N.B. Values <1% not shown

Fig. 4(c): Cumulus humulis: Frequency Distribution.

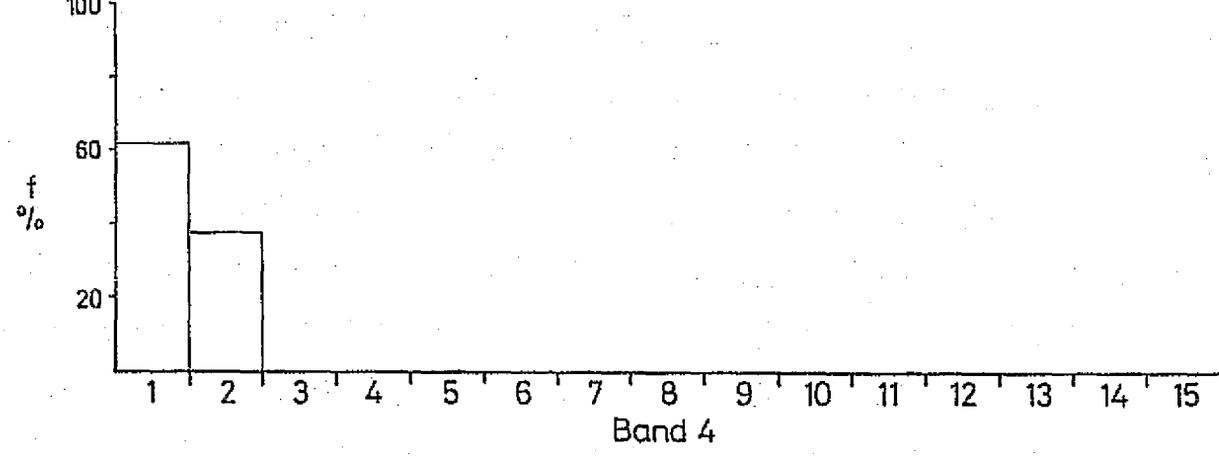

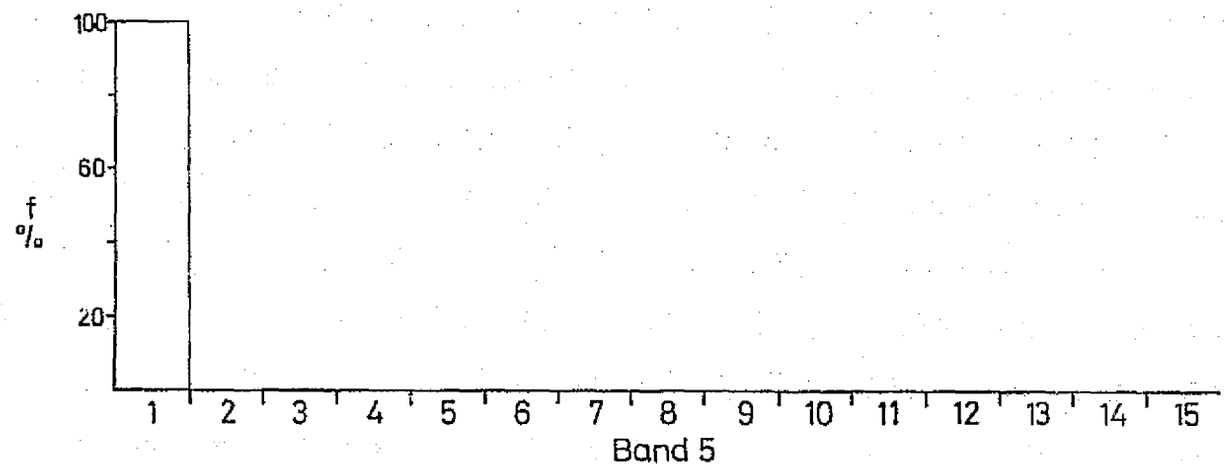

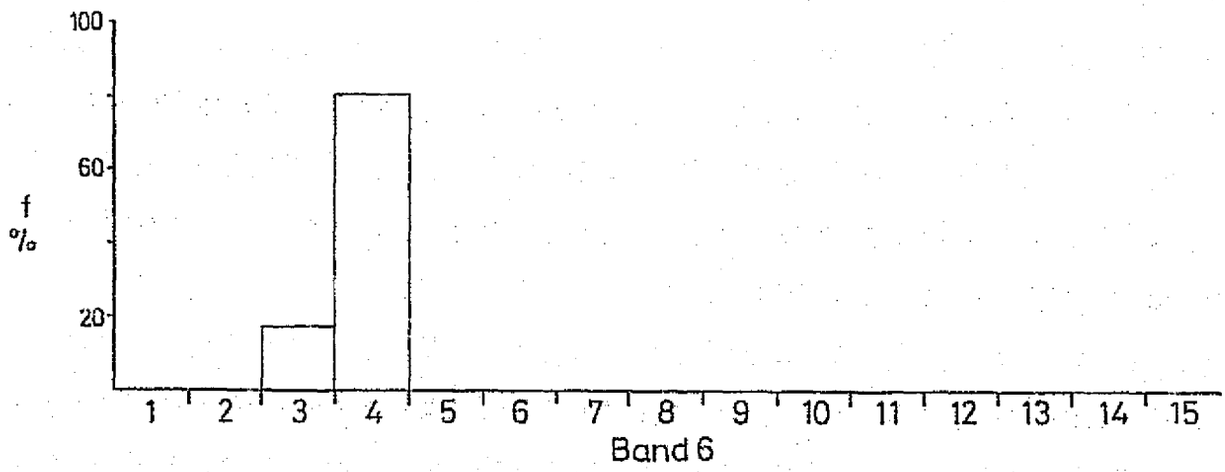

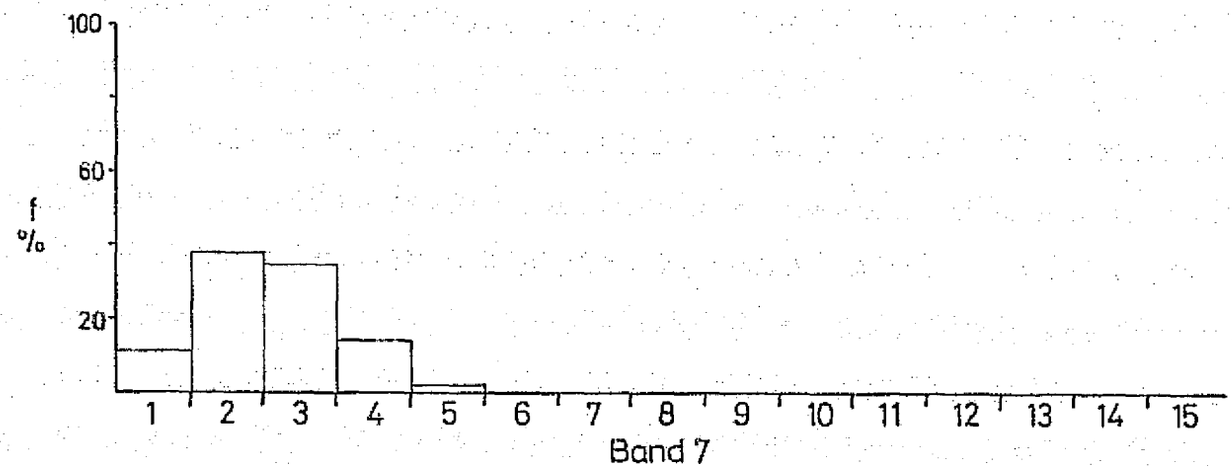

N.B. Values <1% not shown

Fig. 4(d): Stratiform: Frequency Distribution.

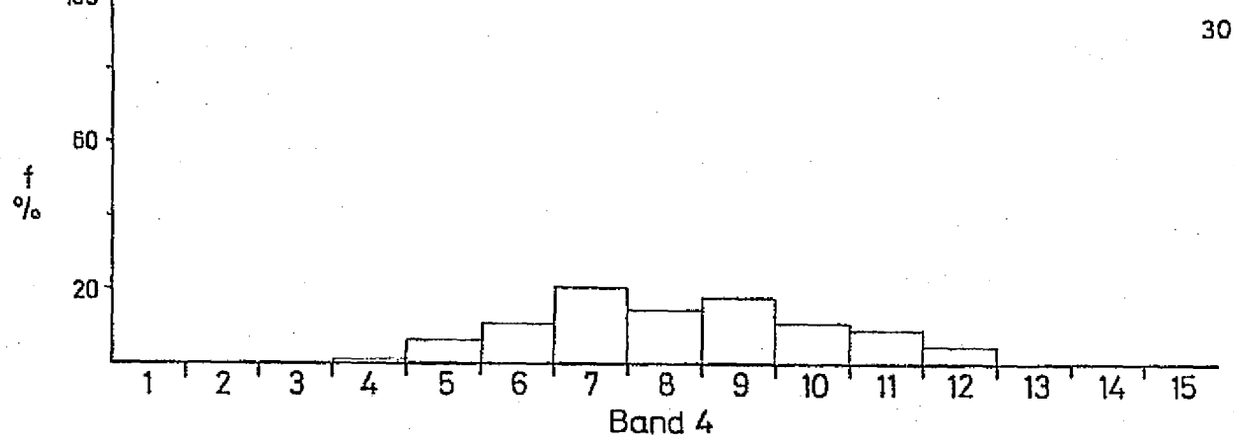

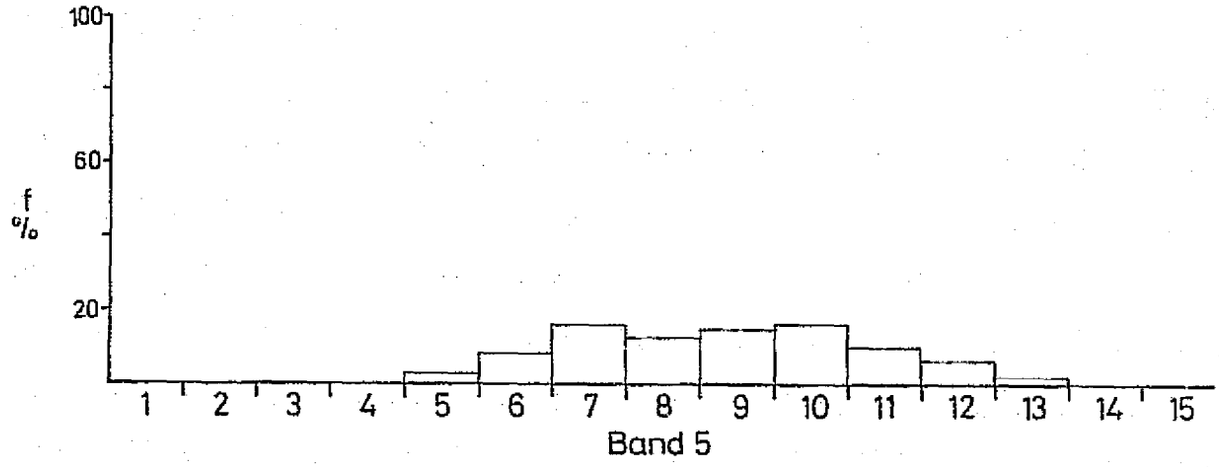

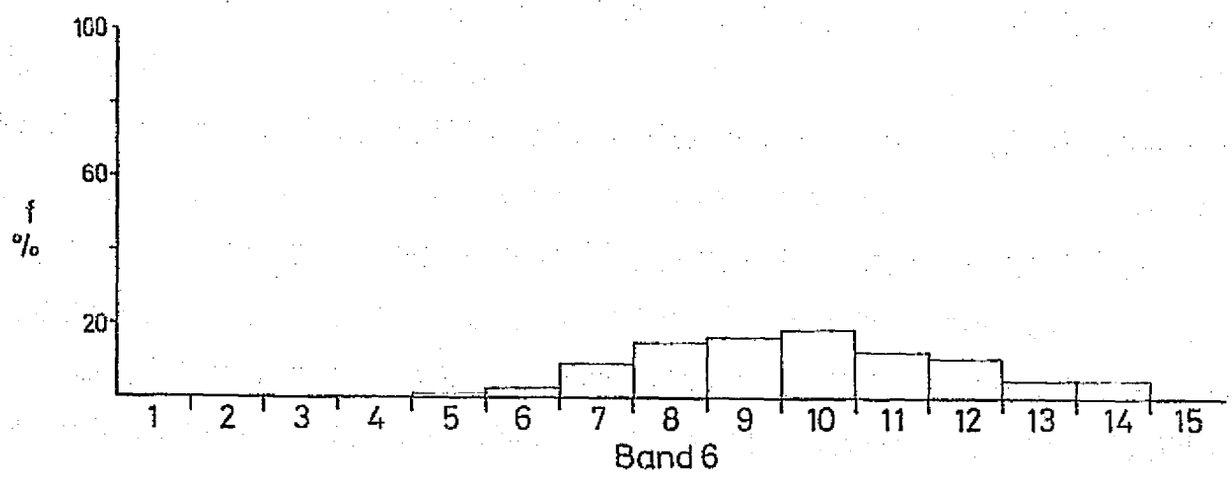

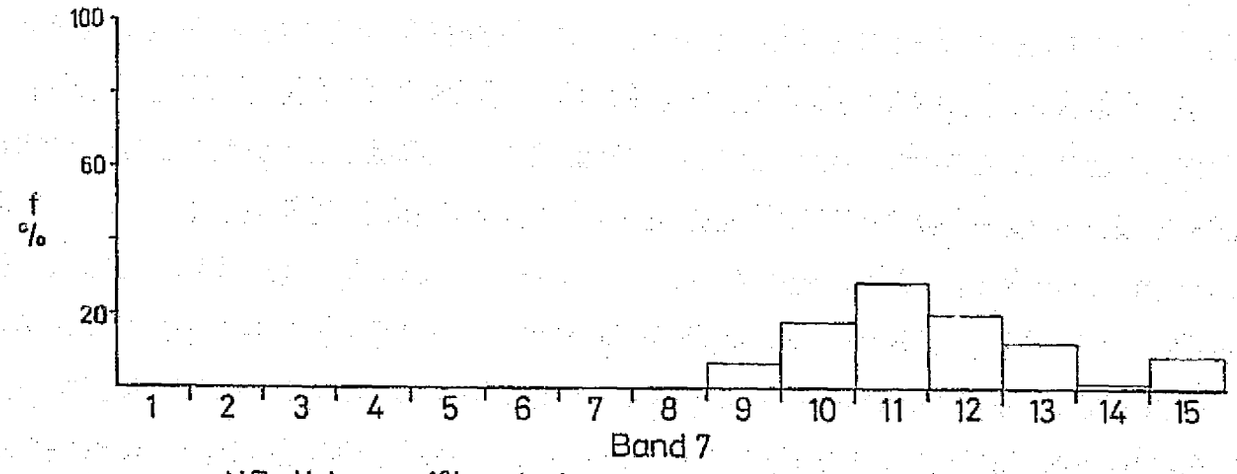

N.B. Values <1% not shown

Fig. 4(e): Stratocumuliform: Frequency Distribution.

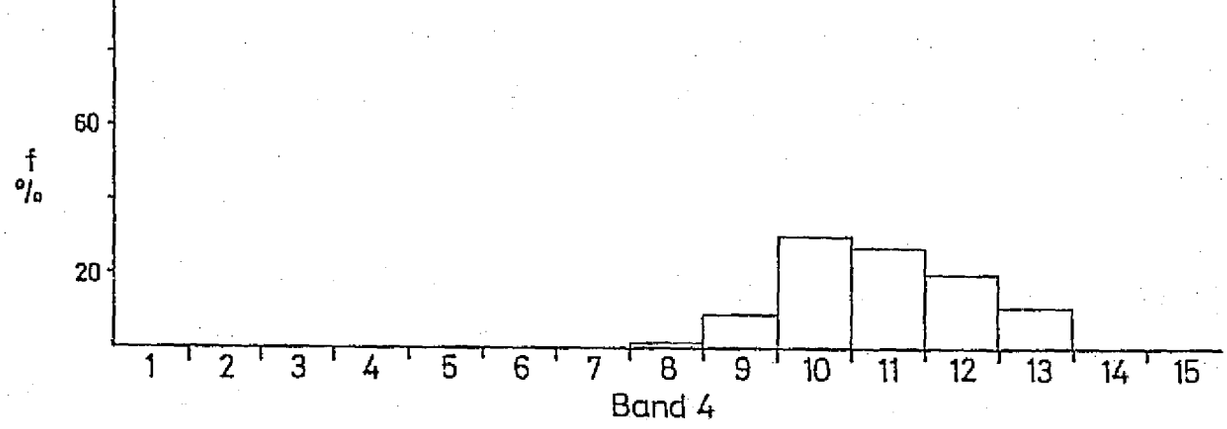

Band 4

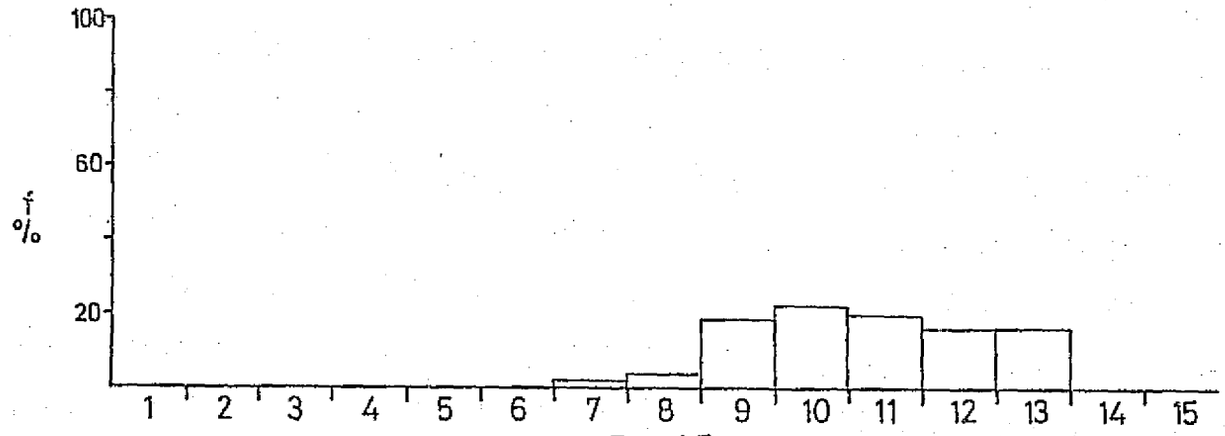

Band 5

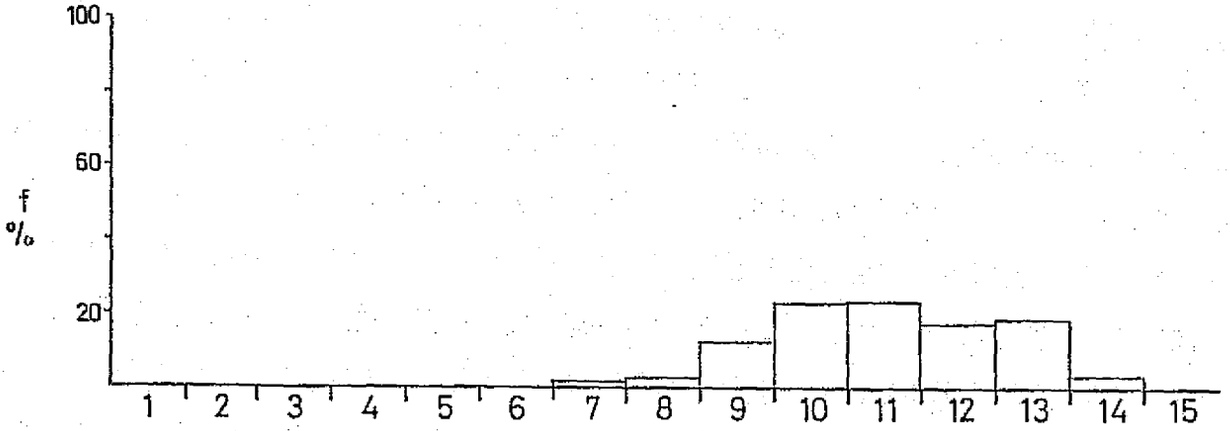

Band 6

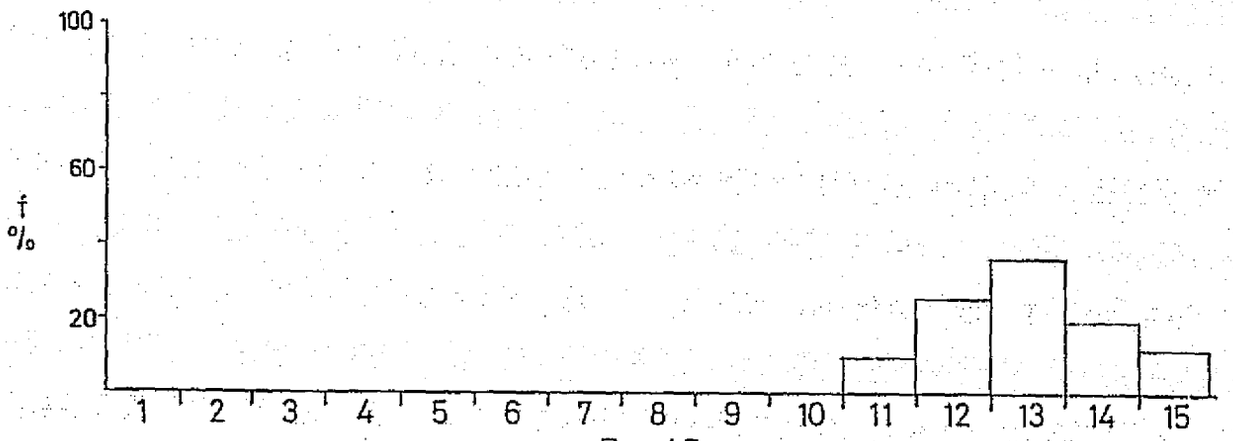

Band 7

N.B. Values <1% not shown

Fig. 4(f): Cirriform: Frequency Distribution.

gently in the centre of the scale. In band 6 there is a slight displacement towards the dark end of the scale. In band 7 there is a significant displacement towards the darker end of the scale, and the range of values is more restricted.

f) Cirriform (Fig. 4(f)): Bands 4, 5 and 6 are similar to one another, with distributions located in the darker portion of the scale and a fairly wide range of values (over 8/9 steps). Band 7 possesses a marked displacement towards the dark end of the scale and the range of values is limited to the darkest 6 steps.

Figs. 4(a)-(f) reveal, therefore, that differences in brightness occur both between the wavebands for individual cloud types as well as, more strikingly, between similar wavebands for different cloud types. To facilitate the examination of these differences, cumulative frequency distributions were plotted. (See Figs. 5(a)-(d)).

These graphs consist of plots of percentage cumulative frequency on an arithmetic probability scale, against image density on an arithmetic scale. First, the average density of each step was found. In the case of step 1 the average density was found by determining the average density range of steps 2 to 5 inclusive. This value was then halved, and subtracted from the upper limit value of step 1 to provide an average value for the brightness of that step. The advantage of using arithmetic probability paper in this analysis is that if the distributions plotted are normal, then a straight line will occur on the graph. A brief examination of these diagrams shows that the distributions were not normal. The chief points that emerged from this analysis were as follows:

a) Band 4 cumulative frequency distributions (Fig. 5(a)). Here stratiform and cumulonimbiform clouds appear to give similar results, both having the majority of their values at the bright end of the scale. Similarly cirriform and stratocumuliform clouds are similar to each other, their curves lying close together

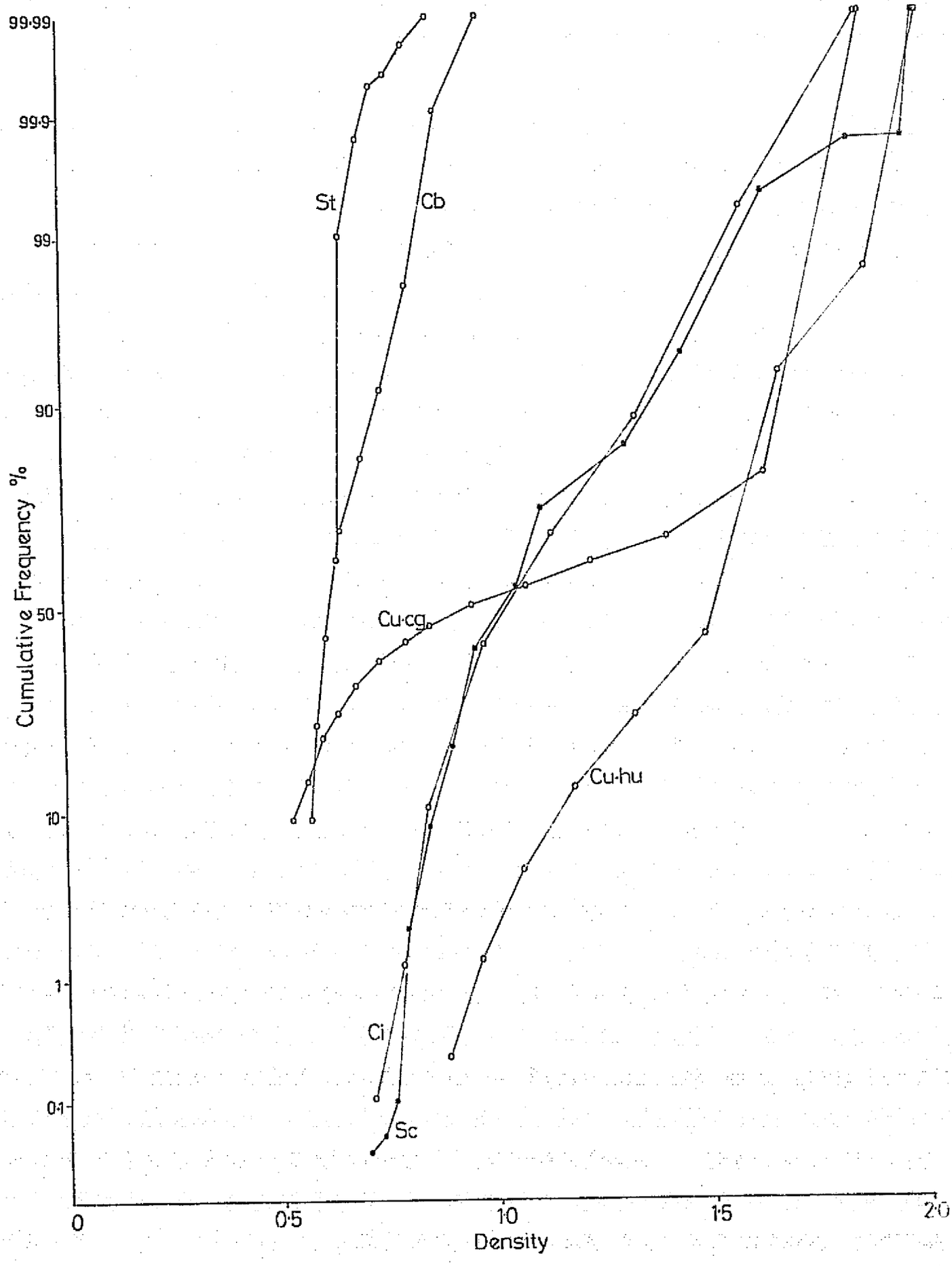

Fig. 5(a): Band 4 Cumulative Frequency Distributions.

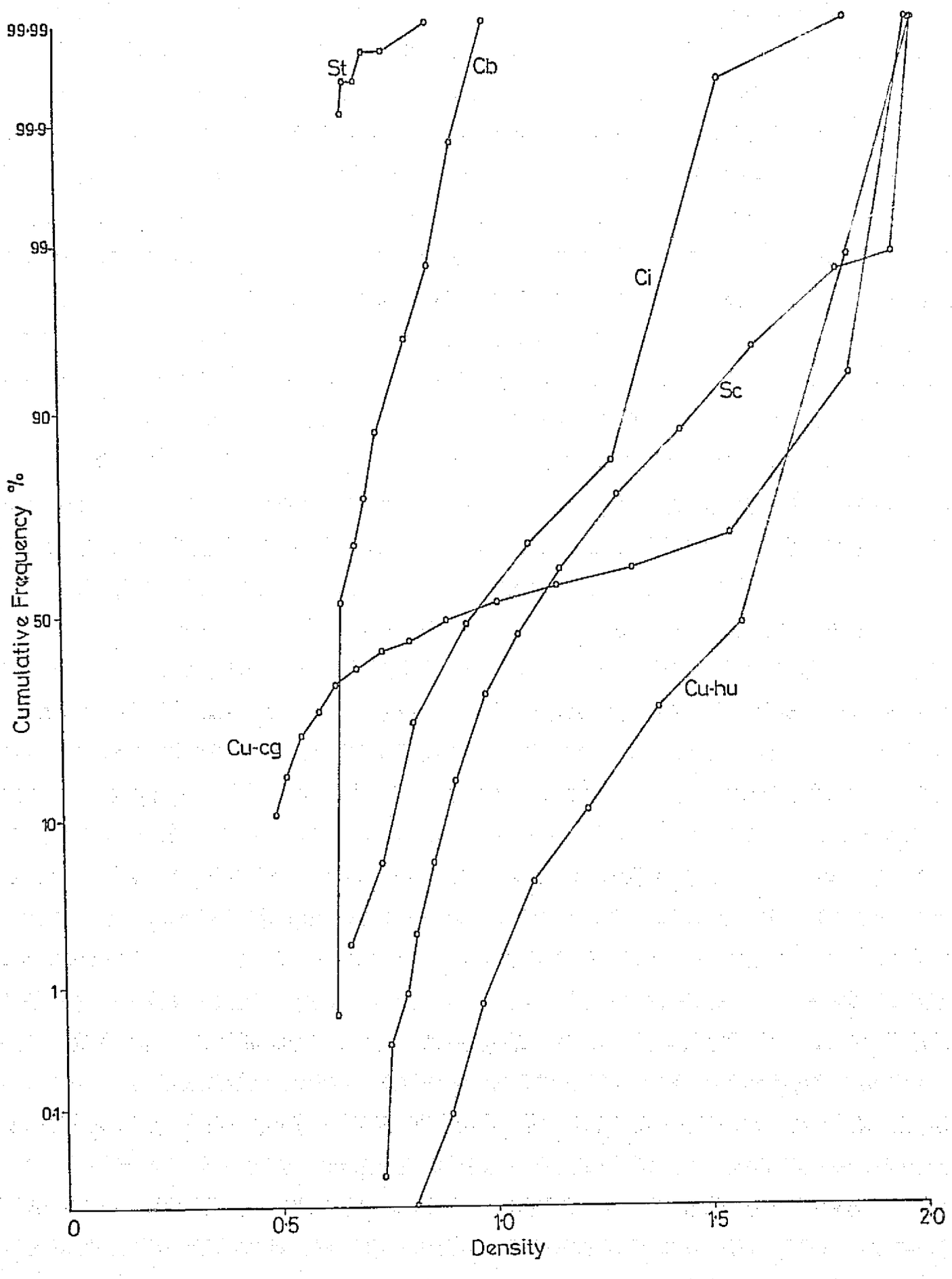

Fig. 5(b): Band 5 Cumulative Frequency Distributions.

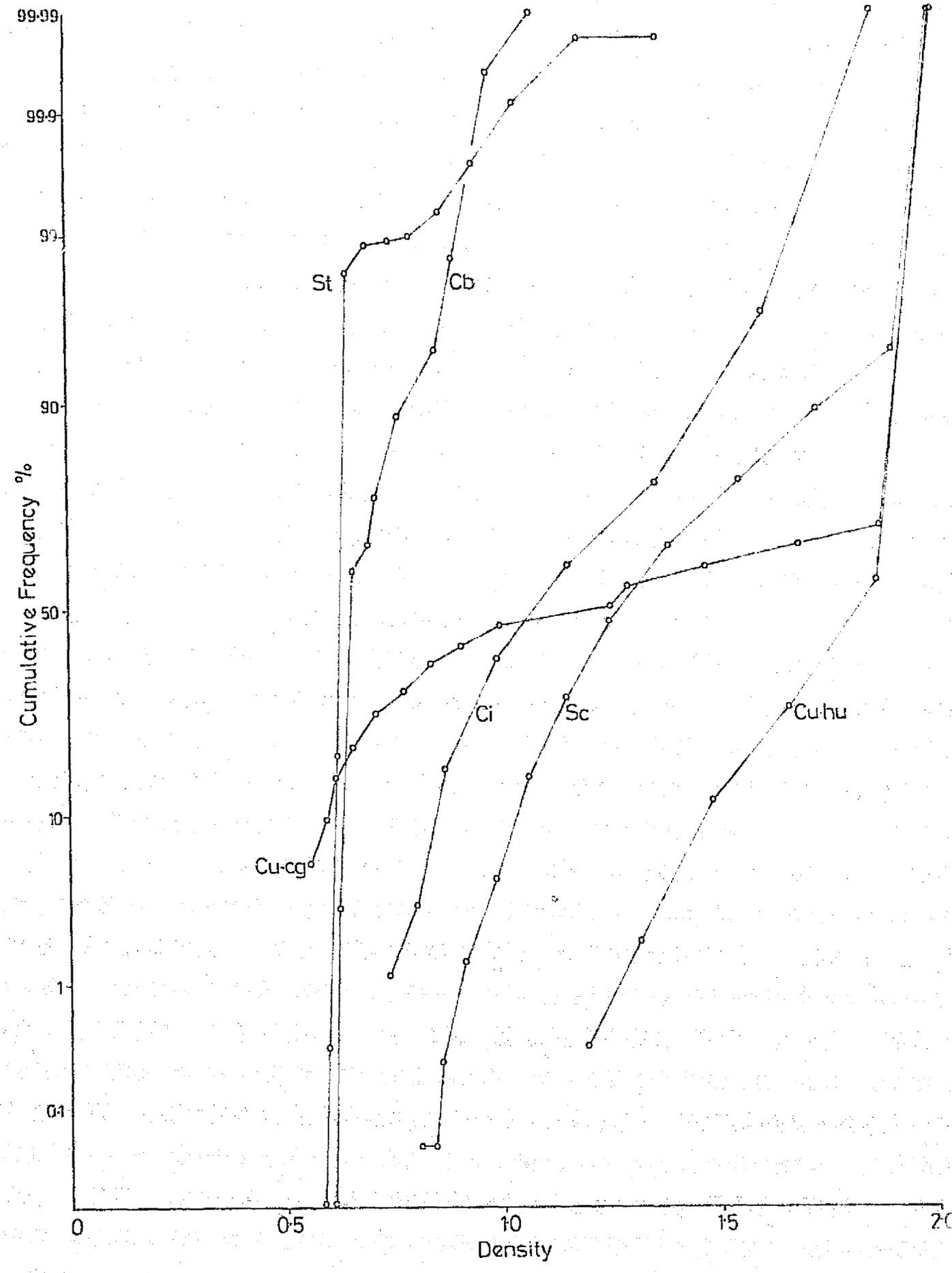

Fig. 5(c): Band 6 Cumulative Frequency Distributions.

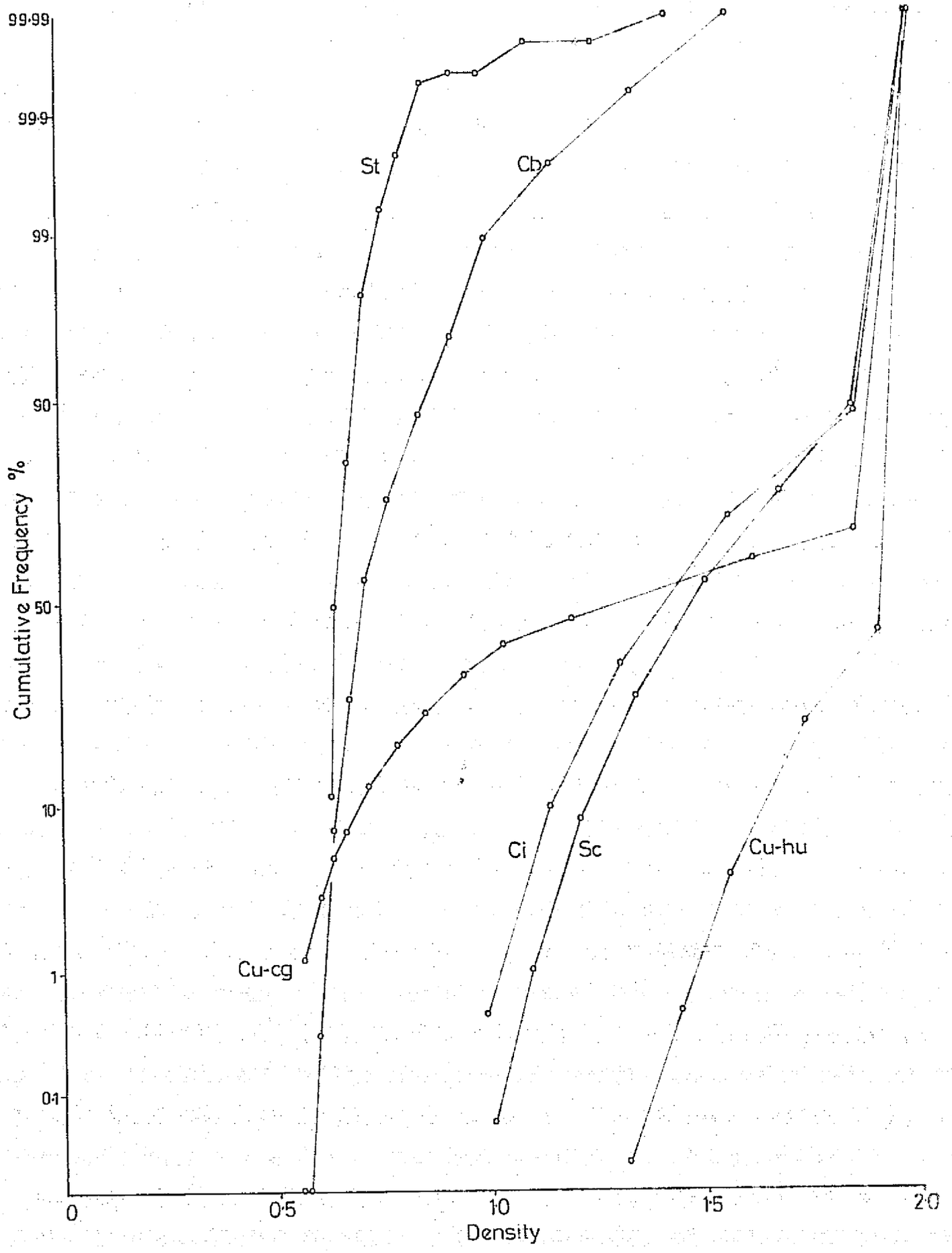

Fig. 5(d): Band 7 Cumulative Frequency Distributions

across much of the graph. At first sight this may appear strange as the graphs of their respective frequency distributions (Figs. 4(e) and 4(f)) apparently revealed considerable differences. However, when one examines Fig. 3, it can be seen that stratocumuliform grey-scale values are considerably brighter than corresponding cirriform values. This is taken into account more fully in Fig. 5(a) where actual density values are employed on the abscissa, not grey-scale step numbers as in Fig. 4. Generally, most cloud types follow paths which are roughly parallel over much of the scale in Fig. 5. The most notable exception to this is cumulocongestus. The plot for this cloud category starts well to the left of the graph and generally rises less steeply than those for the other cloud types except at the dark end of the scale. The tendency for this cloud type then, is for its plot to cut across the plots for cirriform, stratocumuliform and cumulus humilis.

b) Band 5 cumulative frequency distributions (Fig. 5(b)): These are essentially similar to the band 4 plots in Fig. 5(a). However, the stratiform curve is shorter due to the clustering of its values at the bright end of the scale. The cumulus congestus curve again lies across those for the other types.

c) Band 6 cumulative frequency distributions (Fig. 5 (c)): For the first time stratiform extends into darker portions of the scale than does cumulonimbiform. Stratocumuliform is now markedly displaced towards the dark end of the scale in comparison to cirrus. Cumulus humilis is similarly displaced towards darker levels, although it retains its approximately parallel position with respect to cirriform and stratocumuliform. Cumulocongestus intersects the other distributions at quite large angles, as in bands 4 and 5. At the dark end of the scale,

the final 30% of its distribution follows a similar path to that of cumulus humilis.

d) Band 7 cumulative frequency distributions (Fig. 5(d)): In this waveband, cumulonimbiform has been displaced quite markedly towards the dark portion of the scale. The whole of its curve is on the darker side of the stratiform curve. Cirriform and stratocumuliform distributions now follow very similar paths, both having been displaced markedly towards the darker portion of the scale than in band 6. Cumulus humilis is darker than in band 6. This is probably due to the darkening of the sea background which comprises a larger proportion of this image between the small cumulus cells. This effect is also seen in the case of cirriform and stratocumuliform, both of which contain some areas of sea in the imaging area.

These diagrams, Figs. 5(a)-(d), show that marked differences in reflectance characteristics do occur between cloud types and that these differences change from one waveband to another. It is thought that such differences are indeed due principally to target characteristics, not processing practices, for more account is taken of the grey-scale differences in these diagrams through the use of the actual density values of the steps rather than their numbers in the grey-scale.

3. Brightness characteristics of six categories of clouds. summary statistical results

In addition to such graphical descriptions of the brightness frequency distributions, it is possible to gain further insight into the nature of cloud differences by deriving summary statistics via the method of moments. This is a computational method; the analysis of the mean and standard deviation was carried out on the PDP 11/45 mini-computer. Skewness and kurtosis coefficients were determined on a Hewlett-Packard calculator

from the frequency distributions derived by the PDP 11/45. The results of the computations are presented in Table 2.

There are some interesting differences between the summary statistics and the impressions gained of the distributions presented in Figs. 4(a)-(f). For example, the cumulonimbiform statistics show that the kurtosis ("peakedness") of the distributions increases steadily from band 4 through to band 7. An examination of Fig. 4(a) alone would probably have led one to conclude that bands 5 and 6 were more "peaked" than either bands 4 or 7. Cumulocongestus clouds show relatively large standard deviations, a fact less unexpected when Fig. 4(b) is examined. A small negative skewness value is noted in band 7 which corresponds to the increased frequency of values at the dark end of the scale (step 15). The cumulus humilis distributions (Fig. 4(c)) are asymmetrical in nature and this produces negative skewness values for all wavebands. Mean brightness values show a similar trend in all the cloud types. Generally, the mean brightness of each successive waveband is slightly darker than the preceeding waveband. There are two exceptions to this general rule. Both occur in waveband 5 in the cirriform and stratiform cloud types. Such a decrease in brightness with waveband is probably explained by the decreasing brightness of the background area (the sea) with successive wavebands.

Besides this slight anomaly in the general trend of mean brightness values, stratiform clouds also present some other noteworthy summary statistics. The skewness values recorded are very large, indicating extreme asymmetry of the distribution. This is perhaps not surprising when Fig. 4(d) is examined, especially with respect to band 5. However, the kurtosis values seem excessively high when one considers that in sediment analysis values of kurtosis greater than 3.00 indicate extreme leptokurticity (peakedness) and are uncommon.

TABLE 2

Cloud Type	Waveband Number	No. of Data Points	Mean	S.D.	Skewness	Kurtosis
Cumulonimbiform	4	9215	0.65	0.07	1.09	4.13
	5	9215	0.69	0.06	1.75	5.94
	6	9215	0.71	0.07	1.78	6.02
	7	9215	0.76	0.10	1.90	10.05
Cumulus congestus	4	8084	1.13	0.49	0.27	1.46
	5	8084	1.17	0.58	0.22	1.35
	6	8084	1.23	0.57	0.09	1.31
	7	8084	1.40	0.52	-0.09	1.39
Cumulus humilis	4	9025	1.55	0.22	-0.70	3.07
	5	9025	1.63	0.23	-0.82	2.54
	6	9025	1.85	0.19	-1.17	3.44
	7	9025	1.92	0.12	-1.53	4.52
Stratiform	4	8272	0.63	0.01	1.62	13.44
	5	8272	0.57	0.01	50.95	2789.26
	6	8366	0.64	0.04	10.87	168.44
	7	8366	0.66	0.04	3.03	45.02
Stratocumuliform	4	9100	1.12	0.22	0.79	3.21
	5	9100	1.20	0.26	0.87	3.29
	6	9100	1.40	0.28	0.55	2.35
	7	9100	1.59	0.23	0.17	2.08
Cirriform	4	7896	1.14	1.14	0.63	2.71
	5	7896	1.09	1.09	0.49	2.09
	6	7896	1.21	1.21	0.49	2.26
	7	7896	1.57	1.57	0.10	1.96

4. Spectral reflectance graphs for six categories of clouds

The results summarised in sections (1) - (3) above are all related to characteristics of cloud fields viewed over areas of about 33.7 km^2 on the ground. It would be interesting to investigate the degrees of similarity between those results and others for a range of smaller areas. Whilst we must be cautious not to read too much into the results obtained, it seems legitimate to attempt to interpret them in terms of what they may indicate concerning the characteristics of cloud elements viewed by the microdensitometer over areas of about 337m^2 on the ground. Taking the modal classes in Figs. 4(a)-(f) to indicate the most representative brightness values for each cloud category in each waveband we have compiled a set of spectral reflectance graphs for the six cloud examples (see Figs. 6(a)-(f)). It appears therefrom that the spectral reflectance signatures for different categories of clouds possess some marked differences both in form and position on the axes. Not surprisingly the cumuliform and cumulocongestus curves are generally similar, whilst the stratiform and cumulonimbiform curves are disappointingly alike.

It would seem well worthwhile investigating the multispectral differences of Landsat-imaged clouds more carefully, perhaps through the use of digital data from the CCTs so that the full resolution of the imagery might be employed and picture processing problems thereby eliminated.

5. Discussion

It is in the field of sedimentary petrology and geology that this type of statistical analysis has reached its greatest sophistication. The technique of moment analysis has been used to identify and differentiate sediments (e.g. Folk and Ward, 1957) and in the interpretation of the depositional histories of different sediments (e.g. Greenwood, 1972). Generally, bivariate plots have been employed, with each of the four summary statistics being plotted in turn against each of the others.

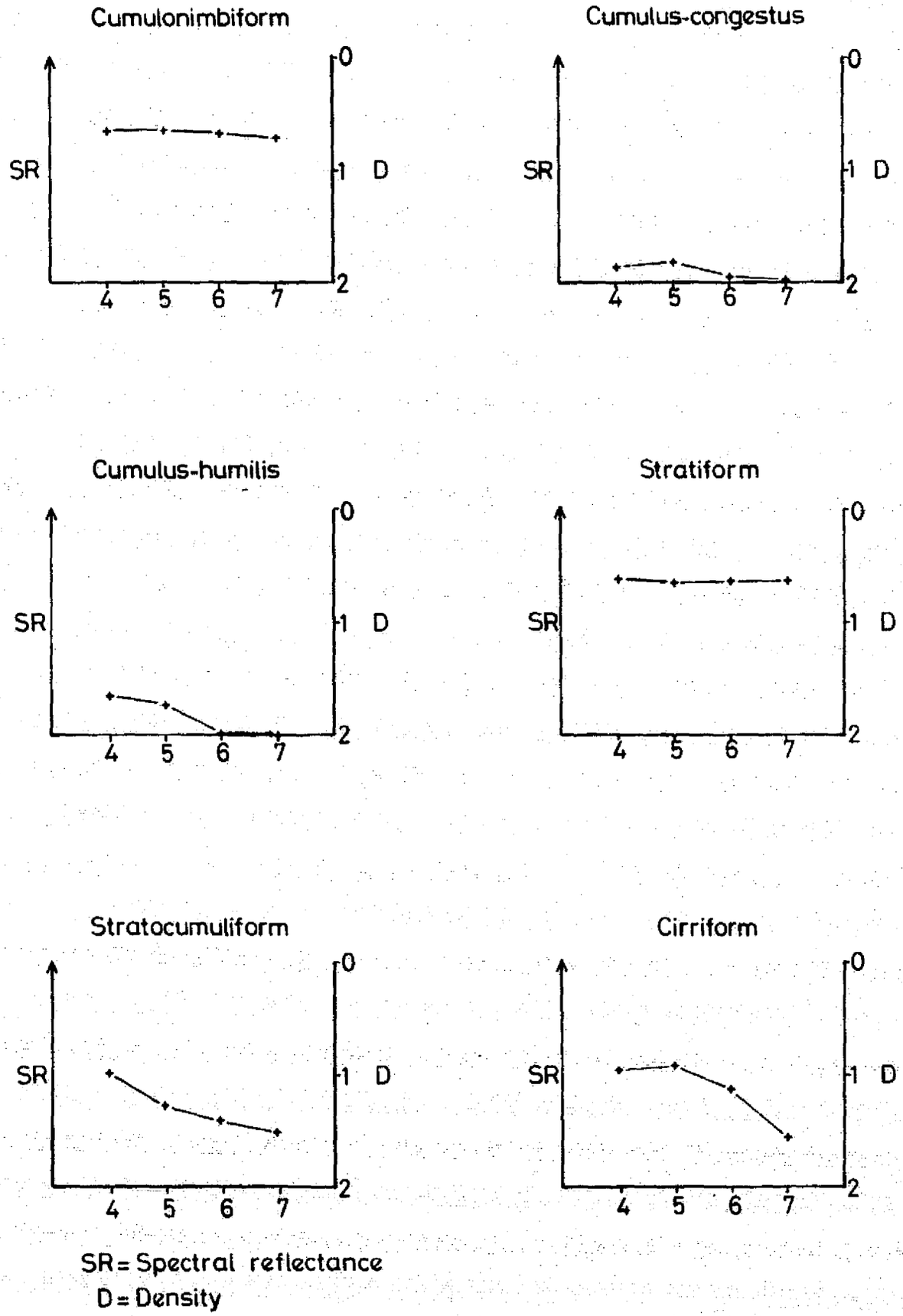

Fig. 6: Spectral Reflectance Graphs.

However, Folk and Ward (1957, p. 23) managed to produce a four-variate graph to represent the relationships between the four summary statistics in one diagram. Often, the analysis of such data has been extended by using clustering and discriminant analyses as classification procedures to allow new data values to be assigned correctly to previously determined groupings.

It is felt that this latter type of analysis may prove most useful in attempts to assign new cloud information in Landsat data to previously determined cloud types, defined in terms of their moment statistics. However, some problems would have to be solved before this were to be possible. For example, our results for stratiform clouds indicate that the application of such techniques to non-normally distributed data without some prior transformation can lead to misleading, possibly erroneous, results and conclusions. One solution might be to transform the data after initial statistics had been calculated. For example, Folk and Ward (1957) produced a transformed kurtosis statistic (K') derived from the ordinary kurtosis value, (K). The relationship is as follows:

$$K' = \frac{K}{(K + 1)}$$

If this transformation had been applied in our study, the range of kurtosis values would have ranged from about 0.5 to 1.0, much less than the range we found. This transformation produces an approximately normal kurtosis distribution (Folk and Ward, 1957, p. 15).

A further problem with our distributions is that at the brightest end of the scale they are "open-ended": no lower limit was defined. Folk (1965), in discussing grain size analyses of sediments, felt that the application of the method of moments to such open-ended distributions might not be justified. This may be pertinent to our extreme results for stratiform clouds, where likely saturation of the image caused many values to be located in the unbounded step 1 of the grey-scale step-wedge.

It is apparent, therefore, that considerable work remains to be done if a worthy aim is to produce an operational cloud identification scheme for Landsat-type imagery based on cloud brightness statistics. However, the difficulties should not prove insurmountable if careful thought is given to experimental design and operation.

IV ACCOMPLISHMENTS

Analysis of sample multispectral images for six different categories of clouds have revealed marked differences between the reflectance characteristics of clouds and cloud fields or cloudy areas in the visible/near infrared region of the electromagnetic spectrum. Although the results obtained so far relate only to clouds imaged over coastal waters of the British Isles in summer the method by which the results were obtained could be applied quickly and cheaply to the analysis of further images.

V PROBLEMS

Several problems of note were encountered in this stage of our ERTS Follow-on Programme Study. These included:

1. Processing problems

These were of two different kinds, namely those already discussed at some length related to evident variations in the processing of Landsat imagery by NASA, and those related to the equipment available to us for image analysis. The two are interconnected in the sense that the poor quality of the copy negatives provided by NASA (see Barrett and Grant, 1975a p.8) determined that we should use the 70 mm positive transparencies obtained from the same source for the microdensitometry investigation, despite their small size for this purpose, rather than enlarged positive transparencies generated from our archive of 70 mm negatives. Since the Optronics Photoscan has a limited number of spot

sizes for image analysis our unit areas represented a larger area on the ground than we would have liked.

2. Interpretation problems

It did not appear that we could satisfactorily disentangle the different and variable influences of picture processing and cloud characteristics in order that we might, with reasonable confidence, assess the cloud differences for their statistical significance. Consequently we have expressed our interpretation of our results only in qualitative terms.

3. Schedule problems

In view of the wide-ranging nature of our project we may be unable to devote as much time to the theme of this report as its theme deserves. However, we hope to apply the methods developed here to some further images for two purposes:

a) To obtain further information on the relations between the unit sizes of the areas measured by the microdensitometer and the brightness characteristics of the clouds and cloudy areas; and

b) To test the similarity between such brightness characteristics for similar cloud fields viewed under contrasting solar illumination conditions, e.g. around the summer and winter solstices.

VI DATA QUALITY AND DELIVERY

Our inability to produce useful positives from the 70 mm negatives received from NASA continues to affect our work adversely. Test positives developed from these negatives have been of a lower quality than those we have produced by copying the 70 mm positives onto contact negatives and then developing these. We are not sure why this should be the case.

Delivery of imagery seems to have slowed further as our project

period has passed. We are still awaiting imagery for March 1976 at the time of writing (mid-August 1976). This has had some effects upon the sequence of work in our study; some of these effects were alluded to in the Introduction to this Report.

VII RECOMMENDATIONS AND CONCLUSIONS

Although the assessment of the brightness characteristics of clouds imaged multispectrally by Landsat is a worthy topic of enquiry in its own right, much of our interest in this matter stems from our broader work in the Applied Climatology Laboratory of the Department of Geography in the University of Bristol. This is concerned with the search for an automatic (objective) method for cloud image analysis and cloud recognition, in relation to a wide range of potential areas of application. The most direct methods of objective cloud mapping include:

a) Brightness contour mapping, as practised with both visible and infrared imagery in the Applications Branch of the National Oceanic and Atmospheric Administration, Camp Springs, Md.;

b) Brightness/texture analysis, a basis for which has been developed in this Department (Harris and Barrett, in preparation);

and c) Multispectral image analysis, summarised by Shenk, Holub and Neff (1976).

The first of these would be difficult to develop into an operational cloud recognition method because of the ambiguity which is evident in contour maps prepared from either visible or infrared imagery when relationships between image brightness and cloud type are considered. For example in visible imagery moderately thick low to middle level stratified cloud may be difficult to distinguish from thick alto- or even cirrostratus; these cloud types (and others) all reflect incident radiation strongly. In infrared imagery deep convective cloud can give brightness

temperatures as low as those associated with deep layered cloud. At best such a method would be an enhancement technique associated with which there would have to be some qualitative assessment of the brightness contours in terms of cloud types.

The second is much more attractive in that it employs two criteria rather than one for the objective differentiation of cloud type. Initial tests suggest that brightness/texture distributions for broad areas of cloud can be subdivided quite well into different cloud categories by discriminant analysis. The chief disadvantage of such a method arises from the common sampling method, which subdivides the initial data array into sub-arrays (say 5 x 5 or 6 x 6 picture points apiece) in order that texture measures might be made: texture is essentially a field characteristic, not a point characteristic as is the case with picture brightness. One significant consequence of this is that some of the resolution of the original data is sacrificed in brightness/texture analyses, on which cloud recognition depends. Even then some cloud types may be hard to separate, especially deep, widespread stratiform/layered cloud and large convective cloud masses topped by dense anvils of cirrus.

The third possibility would appear to have an advantage over the first in that a number of cloud responses would be available for each picture element, increasing the possibility that worthwhile cloud identification could be based thereon. It would also appear to have an advantage over the second in that the full spatial resolution of the original picture information obtained from the satellite could be used for cloud mapping and recognition. However, the present Landsat MSS is not ideally suited for such an operation because of the narrowness of its coverage of the visible-infrared region of the electromagnetic spectrum: the addition of a channel in the broad atmospheric window waveband in thermal infrared (as planned for Landsat C) should significantly help to differentiate further the spectral signatures for different categories of cloud; the addition

of a further channel deeper into the infrared region (c. 20-23 μm) might help still more, especially in differentiating between deep layered clouds and cumulonimbus topped by thick cirrus varieties. In their earlier work Barnes and Chang (1968), Greaves and Chang (1970) and Lo and Johnson (1971) concentrated upon rather low resolution weather satellite data when seeking to assess the possibilities of multispectral cloud type identification procedures. Similarly Shenk and Holub (1973) and Shenk, Holub and Neff (1976) based their conclusions on MRIR analysis, and admitted that their proposed Cloud Type Decision Matrix might be expected to work well without further assistance and/or refinement only over tropical oceans. We would like to think that some future satellite system might employ a multispectral sensor system with a daily, global mapping capability and a resolution more in keeping with the present Landsat MSS than the Tiros or Nimbus MRIR - but designed for simultaneous Earth observation/atmospheric assessment purposes. It is probably only in this way that a multispectral cloud identification system could be operated economically in the foreseeable future - economy of effort as well as cost being significant when it is remembered that a brightness/texture cloud identification scheme is well within the realms of practical possibility, this suffering chiefly by comparison on account of the resolution problem.

It would seem that considerable benefits might accrue to all concerned were atmospheric and terrestrial investigators to collaborate more closely in future satellite design and operations: the problems of meteorologists, oceanographers and Earth resource scientists are, perhaps, not only more closely interrelated than is commonly acknowledged, but more amenable to solutions which overlap considerably even though they might not precisely coincide.

ACKNOWLEDGEMENTS

Our thanks are due to NASA for provision of the Landsat imagery, and the U.K. Department of Industry for practical and financial support for our project. We are indebted to Dr. H. Muirhead and Dr. H. Watson of the Molecular Enzymology Laboaratory, University of Bristol for access to the Optronics Photoscan and PDP Computer.

REFERENCES

BARNES, J.C. and CHANG, D. (1968): "Accurate cloud cover determination and its effects on albedo computations", Final Report NAS 5-10478, Concord, Mass., Allied Research Associates, Inc., 82 pp.

BARRETT, E.C. and GRANT C.K. (1975a): "ERTS Follow-on Program Study No. 2962A", Unpublished Notes.

BARRETT, E.C. and GRANT, C.K. (1975b): "Mesoscale assessments of cloud and rainfall over the British Isles", ERTS Follow-on Program Study No. 2962A, First Quarterly Report, NASA-CR-146033, Greenbelt, Md., 27 pp.

BARRETT, E.C. and GRANT, C.K. (1976a): "The identification of cloud types in Landsat MSS images", ERTS Follow-on Program Study No. 2962A, Second Quarterly Report, NASA-CR-146647 Greenbelt, Md., 50 pp.

BARRETT, E.C. and GRANT, C.K. (1976b): "Comparisons of cloud cover evaluated from Landsat imagery and meteorological stations across the British Isles", ERTS Follow-on Program Study No. 2962A, Third Quarterly Report, NASA Greenbelt, Md., 45 pp.

DANKO, J.M. (1974): "Meteorological utility of high resolution multispectral data", Final Report, NASA-CR-138809, Greenbelt, Md., 61 pp.

FOLK, R.L. (1965): "Petrology of sedimentary rocks", Austin, Texas, Hemphill's.

FOLK, R.L. and WARD, W.C. (1957): "Brazos River bar: a study in the significance of grain size parameters", Journal of Sedimentary Petrology, 27, p. 3-26.

GREAVES, J.I. and CHANG, D. (1970): "Technique development to permit optimum use of satellite radiation data", Final Report, N62306-69-C-022, Concord, Mass.,Allied Research Associates, Inc., 102 pp.

GREENWOOD, B. (1972): "Modern analogues and the evaluation of a Pleistocene sedimentary sequence", Transactions of the Institute of British Geographers, 56, p. 145-169.

HARRIS, R. and BARRETT, E.C. (in preparation): "Towards an objective satellite nephanalysis".

LO, R.C. and JOHNSON, D.R. (1971): "An investigation of cloud distributions from satellite infrared radiation data", Monthly Weather Review, 99, p. 599-605.

MILLER, D.B. (1971): "Automated production of global cloud climatology based on satellite data", Technical Report 242, Air Weather Service (MAC), U.S.Air Force, p.291-306.

N.A.S.A. (1971): "Data users handbook", NASA, Greenbelt, Md.

N.A.S.A. (1973): "Proceedings of the NASA Earth Resources Survey Symposium" NASA TM-X-58168, NASA, Houston, Texas.

ROSENFELD, A. (1970): "A non-linear edge detection technique", Proceedings of the IEEE, 58, p. 814-816

SHENK, W.E. and HOLUB, R.J. (1972): "A multispectral cloud type identification method using Nimbus 3 MRIR measurements", Conference on Atmospheric Radiation, Boston, American Meteorological Society, 3 pp.

SHENK, W.E., HOLUB, R.J. and NEFF, R.A. (1976): "A multispectral cloud type identification method developed for tropical ocean areas with Nimbus-3 MRIR measurements", Monthly Weather Review, 104, P. 284-291.